minerals

MDPI

Article

The Evolution of Permian Source-to-Sink Systems and Tectonics Implications in the NW Junggar Basin, China: Evidence from Detrital Zircon Geochronology

Xingyu Chen [1], Zhijie Zhang [2,*], Xuanjun Yuan [2], Li Wan [2], Chuanmin Zhou [2], Yinhe Liu [2] and Dawei Cheng [2]

[1] School of Earth and Space Sciences, Peking University, Beijing 100871, China
[2] Research Institute of Petroleum Exploration and Development (RIPED), PetroChina, Beijing 100083, China
* Correspondence: zhzhijie@petrochina.com.cn

Abstract: The basin type of the Junggar Basin changed during the Permian, but the time constraint of the tectonic evolution remains unclear. Besides, the fan deltas developed in the Permian in the Mahu Sag in the northwestern of the oil-rich basin. However, the provenances of the sedimentary systems remain unclear. Based on petrology and detrital zircon U-Pb ages, this study investigates the source-to-sink systems evolution and tectonics implications. Abundant lithic clasts in sandstones with low compositional and textural maturity imply proximal sources. The dating results showed a dominant peak (310–330 Ma) and a secondary peak (400–440 Ma) in the northern Mahu Sag, only one peak at 295–325 Ma in the central Mahu Sag, several peaks at 270–350 Ma in the southern Mahu Sag, and multiple peaks at 370–450 Ma in the Zhongguai Uplift. Thus, the north-western Junggar Basin was divided into four major source-to-sink systems, with adjacent central West Junggar as the main provenance and northern and southern West Junggar as the secondary provenance. The proportion of sediment supply from the southern and northern West Junggar is higher during the Middle-Late Permian. It suggests that the source-to-sink systems show inheritance and evolve from a single provenance into a complex provenance, indicating the uplift of West Junggar. The tectonic inversion may occur early in the Middle Permian and the response to tectonic activity is stronger in the southern West Junggar than in the northern West Junggar.

Keywords: Junggar Basin; Permian; provenance; U-Pb zircon geochronology; source-to-sink

Citation: Chen, X.; Zhang, Z.; Yuan, X.; Wan, L.; Zhou, C.; Liu, Y.; Cheng, D. The Evolution of Permian Source-to-Sink Systems and Tectonics Implications in the NW Junggar Basin, China: Evidence from Detrital Zircon Geochronology. *Minerals* **2022**, *12*, 1169. https://doi.org/10.3390/min12091169

Academic Editor: Davide Lenaz

Received: 27 July 2022
Accepted: 13 September 2022
Published: 15 September 2022

1. Introduction

Located in the southern part of the Central Asian Orogenic Belt (CAOB) in northwestern China, the Junggar Basin is tectonically complex. Many scholars have extensively studied the stratigraphic stratigraphy, fault system, basin property, and tectonic evolution of the northwestern Junggar Basin at different periods, and have achieved many results. Some scholars believe that the northwest Junggar Basin in the Early Permian was a foreland basin associated with subduction collision [1–3]. As well, some scholars conclude that the northwest Junggar Basin belongs to a rifting basin formed in the post-accretionary orogenic stage [4–6]. There are also controversies about the prototype basin and the time limit of the tectonic evolutionary stage in the northwestern Junggar Basin during the different geological periods. Previous studies have generally concluded that the northwestern Junggar Basin underwent a tectonic transition in the Late Permian [7,8]. However, some scholars argued that the prototype basin was transformed in the Middle Permian [6,9,10].

The properties of prototype basins at different stages lead to different sediment accumulation patterns. The orogenic belt not only controls the basin evolution but also provides a large number of sediments. These sediments, in turn, record important infor-

mation about the history of the orogenic belt. Therefore, provenance analysis can effectively study the coupling relationship between mountain-basin to provide important constraints for restoring paleogeography and tectono-sedimentary evolution, which is one of the critical contents of sedimentary response mechanisms [11,12].

The Mahu Sag is the most important hydrocarbon-rich sag on the northwestern margin of Junggar Basin, whose border is the Zhongguai Uplift (ZU) in the southwest. In 2017, a fan delta conglomerate reservoir was discovered in the Lower Triassic Baikouquan Formation (T_1b) in the Mahu Sag [13,14]. The subsequently discovered multiple coarse-grained fans in the Permian have demonstrated the enormous potential for oil exploration and development [15]. Chinese scholars mostly focus on the planar distribution, depositional characteristics, and reservoir properties of the sedimentary system in the Mahu-Zhongguai area [16–18]. However, only a few studies have investigated the provenances in the Permian, and they only discuss the lithology and tectonic setting of the parent rock. Huang et al. [19] performed the geochemical analysis of the mudstones of the Upper Permian Wuerhe Formation and found that the source rocks are mainly felsic igneous rocks, and the tectonic setting during the formation of source rocks is probably an oceanic island arc. Wei et al. [10] calculated the clastic composition of sandstone and conglomerate using core observation and microscopic statistics. The research concluded that the Permian sediment sources were mainly from the adjacent West Junggar magmatic rocks, and also came from the source supply of denuded and re-deposited materials. Based on seismic profiles, detrital petrology, and zircon U-Pb ages, Tang et al. [20] suggested that volcanic detritus is abundant in Mahu Sag during the Permian and sediment supply was entirely local. During the middle Permian post-rift phase, sediment supply exceeded thermal subsidence, and the distant sources became increasingly important.

Generally speaking, there is a lack of clear definitions of the provenance systems in the Mahu-Zhongguai area, especially the constraints on detrital zircon U-Pb dating. Detrital zircon U-Pb geochronology is a relatively mature method and is widely used for tracing sediment routing systems and analyzing the tectonic evolution of the source area [21,22]. In deep-water exploration areas where drilling wells are lacking, the source-to-sink systems can be used to conduct provenance analysis and stratigraphic studies based on the characteristics of the sedimentary systems. Relatively effective and relatively low-cost information such as mineral components, heavy mineral assemblages, and detrital zircon U-Pb geochronology can be used to reconstruct the paleo-drainage system and the source-to-sink system distribution pattern. This information can also be further applied in reservoir prediction to constrain the reservoir distribution and provide basics for oil and gas exploration and mining prediction. Meanwhile, the location of the study area is very close to the source area, which enables us to reconstruct the Permian tectonic evolution of the northwest margin of the Junggar Basin with higher sensitivity.

In this study, the research target is the Permian source-to-sink system in the Mahu-Zhongguai area on the northwestern margin of the Junggar Basin. The source-to-sink system was traced based on petrology and U–Pb geochronology of detrital zircons. Combined with previously published findings on the lithology and age distribution characteristics of the potential provenance, the source-to-sink system was logically divided. Finally, the evolution of the source-to-sink system and its significance for tectonic evolution were analyzed.

2. Regional Geological Settings

The Junggar Basin is a large, superimposed composite basin formed on the pre-Carboniferous composite basement after long-term activities in the peripheral tectonic zone. During the Carboniferous, island arcs (Zhongguai, Luliang, etc.) were dispersed in the Junggar Ocean to form a multi-island ocean pattern [23]. At the end of the Carboniferous, the arc-basin systems across the entire Junggar area collided and spliced successively, completing the ocean-continent transformation and forming the amalgamated basement of the Permian Junggar Basin [23]. From the Late Carboniferous

to the Early Permian, the Junggar Basin was in the post-collision adjustment period [24,25], and post-orogenic extension led to the extensive development of magmatic rifting events in the Late Carboniferous to the Early Permian [26,27]. From the Late Permian to the Triassic, the northwestern margin of the Junggar Basin was a strong thrust nappe [6,10].

According to magmatism and stratigraphic distribution, West Junggar can be divided into three parts: northern West Junggar (NWJ), central West Junggar (CWJ), and southern West Junggar (SWJ) (Figure 1c) [28,29]. The NWJ is composed of two major magmatic arcs, the northern part is the Zharma-Saur arc (ZhSA) and the southern part is the Boshchekul-Chingiz arc (BCA). These two magmatic arcs are bounded by the east-west Cambrian-Ordovician Kujibai-E'min-Hobokesar-Hongguleleng ophiolitic mélange belt [30–33]. The Late Paleozoic ZhSA is distributed in the Tarbagatai, Saier, and Saur Mountains and is the product of the southward subduction of the Irtysh-Zaysan Ocean in the north during the Late Paleozoic [31,34,35]. The ZhSA develops the sedimentary rocks and intermediate-felsic volcanic rocks in the Devonian [36]; also develops the marine volcano-sedimentary rocks and calc-alkaline intrusive rocks in the Early Carboniferous [37]. Ordovician volcanic strata are locally developed in the western ZhSA [38]. The Early Paleozoic BCA is distributed in the Wuerkashier Mountains, Xiemisitai Mountains, and Sharburti Mountains. The BCA is composed of the Early Silurian arc volcanic rocks, the Middle Silurian-Middle Devonian intermediate-felsic intrusions, and the Silurian-Ordovician marine sedimentation [39,40]. The accretionary complexes in the CWJ are found in the Barleik, Zaire and Hala'alate Mountains, composed of the Devonian Darbut and Karamay ophiolitic mélange belt [41,42] and the Carboniferous-Devonian volcano-sedimentary rocks [43,44]. In addition, there are mainly two periods of magmatic activity in the CWJ, Early Carboniferous and Late Carboniferous-Early Permian respectively [45,46]. The Barleik-Mayile-Tangbale magmatic arc (BMTA) in SWJ is located near Mayile Mountain, composed of Early Paleozoic ophiolitic mélanges, island arc magmatic rocks and pyroclastic sedimentary strata [47,48], while the tectonic unit was intruded by Late Carboniferous-Early Permian granites [49,50]. The accretionary complexes in the SWJ near Barleik Mountain are composed of Carboniferous-Devonian volcano-sedimentary rocks [51,52].

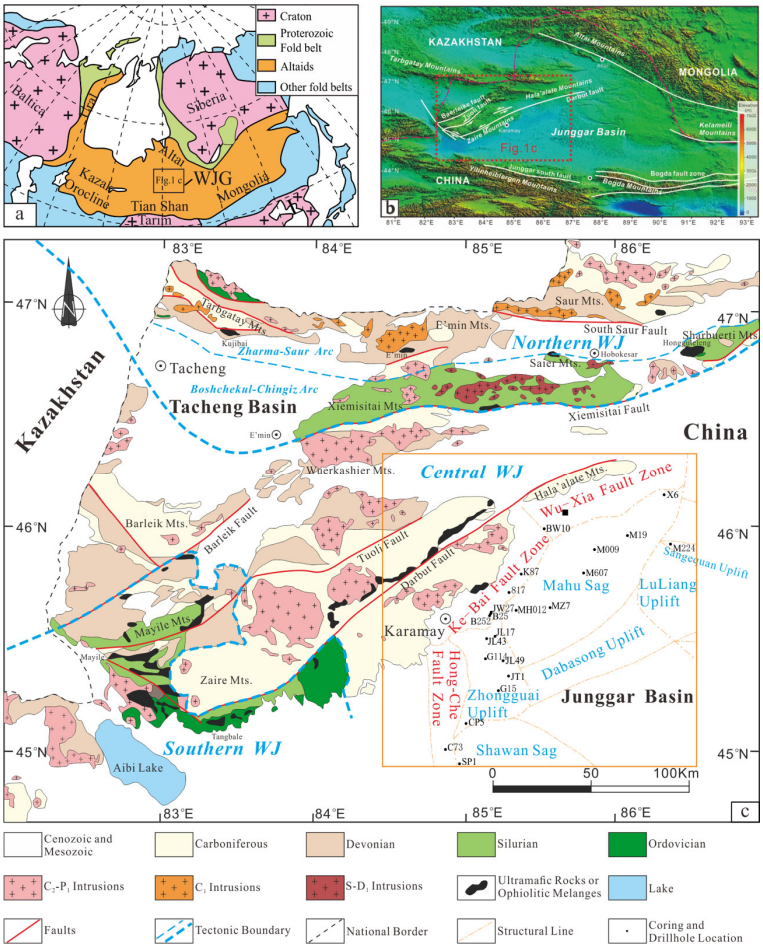

Figure 1. (**a**) Structural diagram of West Junggar and adjacent areas [53]. (**b**) Topographic map of West Junggar and adjacent areas, showing the main faults in the periphery of the basin [44]. (**c**) Geological map of West Junggar [54] and the tectonic unit division map of the northwestern margin of the Junggar Basin (modified according to Xinjiang Oilfield Company). The area inside the orange box is the study area. WJ = West Junggar2. Regional Geological Settings.

The Mahu Sag on the northwestern margin of the Junggar Basin is NNE-trending, with a width of ~50 km from east to west and a length of ~120 km from south to north [9]. The Permian strata are sequentially overlain by the lower Permian Jiamuhe Formation (P_1j), the Fengcheng Formation (P_1f), the Middle Permian Xiazijie Formation (P_2x), the Lower Wuerhe Formation (P_2w), and the Upper Permian Upper Wuerhe Formation (P_3w) [55] (Figure 2). The lower part of the Lower Permian Jiamuhe Formation is mainly characterized by the development of multistage intermediate-mafic volcanic rocks [56]. The Fengcheng Formation is characterized by alkaline lake sedimentation [57–59], with the development of fine-grained argillaceous rocks and dolomitic rocks [60], which are the most important source rocks [61]. The Middle Permian Xiazijie Formation is characterized by glutenite deposits, developing the near-source fan delta sedimentary system [62,63]. The overlying Lower Wuerhe Formation contains more middle- and fine-grained deposits. The main sedimentary facies associations are recognized: the fan delta and the shallow lake [64,65]. The Upper Permian Upper Wuerhe Formation developed an alluvial fan system at the basin margin, which transitioned into a fan delta and littoral-shallow lacustrine facies associations towards the lake [66–68] (Figure 3). The strata of the northern Mahu Sag (NMS) were not well preserved due to denudation after thrust faulting [69–71].

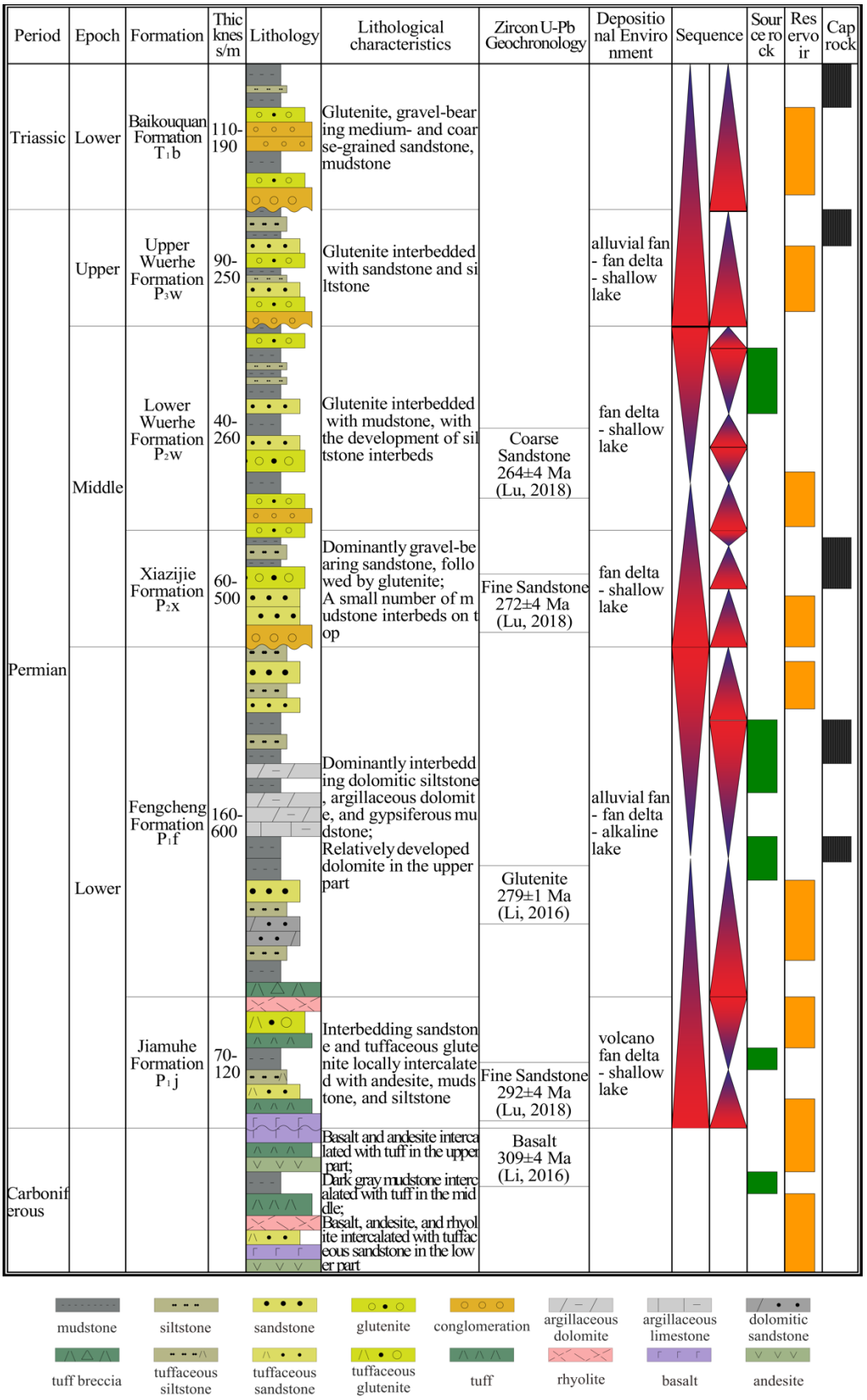

Figure 2. Generalized stratigraphic columns of the studied Permian series. See text for series descriptions and zircon geochronology [72,73]

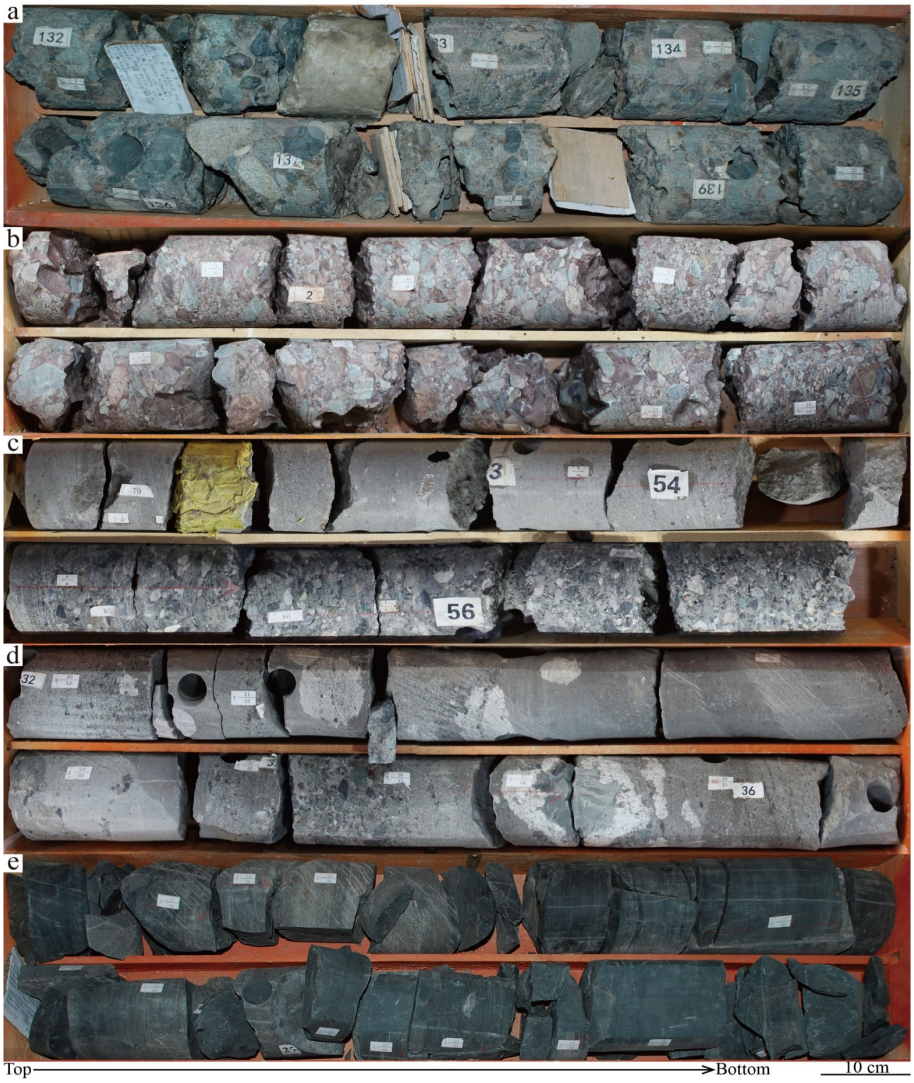

Figure 3. Core characteristics of (**a**) alluvial fan (JL42, 2892.52-2895.34 m), (**b**) fan delta plain (MH25, 3695.36-3697.36 m), (**c**) proximal fan delta front (J206, 4068.55-4070.44 m), (**d**) distal fan delta front (MH20, 4241-4242.86 m) and (**e**) shallow lake (JL49, 4547.84-4549.5 m) deposits.

The characteristic of the alluvial fan is random arrangement conglomerate with coarse cobble, poor sorted, and matrix supported, indicating gravity current (Figure 3a). The fan-delta plain deposits in the distal, subaerial part of the alluvial fan, including gravity flow and traction flow deposition. Facies consist of brown matrix-rich supported conglomerate, cross-bedding or parallel-bedding conglomerate and coarse sandstone, massive conglomerate and sandstone, and clast-supported channelized conglomerate with middle sorted (Figure 3b). The fan-delta front is dominated by large-scale subaqueous deposition both in the proximal and distal. The facies comprise: distributary channel sandstone and clast-supported conglomerate with well sorted, grey-green cross-bedding or parallel-bedding conglomerate and sandstone, structureless sandstone, and siltstone (Figure 3c,d). The lacustrine facies association is composed of dark grey structureless to horizontal lamination siltstone and claystone (Figure 3e).

3. Materials and Methods

3.1. Sample Collection

A total of 26 rock samples were collected from five different Permian formations in the Mahu-Zhongguai area to trace the provenance of the northwestern margin of the Jung-

gar Basin and reconstruct its evolutionary history (see Figure 1c and Table 1 for the sampling locations and formations). Because there is no Permian outcrop on the northwestern margin, all the samples were collected from a drilling core. The dominant lithology is sandstone. Glutenite and conglomerate were collected for zircon U–Pb geochronology in the formations with no sandstone deposition.

Table 1. Information on samples used for laser ablation inductively coupled plasma mass spectrometry dating of detrital zircons in the Mahu-Zhongguai area on the northwestern margin of the Junggar Basin

Sample ID	Well ID	Depth (m)	Formations	Lithology	Number of Dating Zircon Grains	Number of Effective Zircon Grains
MH012-01	MH012	3604.69	P_3w	Silty fine-grained sandstone	100	70
B252-4	B252	2915.8		Muddy fine-grained sandstone	100	67
JL43	JL43	3116.2		Medium- and coarse-grained sandstone	80	65
JT1-2	JT1	4483.22		Medium- and fine-grained sandstone	79	71
CP5	CP5	4350.95		Pebbly medium- and coarse-grained sandstone	80	70
SP1-2	SP1	4828.53		Pebbly coarse-grained sandstone	80	56
X6-2	X6	3263.63	P_2w	Pebbly medium- and coarse-grained sandstone	80	75
M19	M19	3783.32		Pebbly medium- and coarse-grained sandstone	81	71
M224	M224	4206.2		Conglomerate	80	76
BW10-2	BW10	2660.44		Medium- and fine-grained sandstone	80	70
M009	M009	3786.3		Medium- and coarse-grained sandstone	80	64
M607	M607	4101.94		Medium- and fine-grained sandstone	80	63
MZ7	MZ7	4465.6		Fine-grained sandstone	80	72
MH012-2	MH012	4019.6		Medium-grained sandstone	80	77
JW27-12	JW27	3255.5		Pebbly medium- and fine-grained sandstone	99	83
JL17-01	JL17	3602.6		Pebbly medium- and coarse-grained sandstone	94	73
G114-04	G114	3300		Medium- and fine-grained sandstone	97	86
C73	C73	4135.65		Conglomerate	80	67
JL49-01	JL49	4548.4	P_2x	Medium- and coarse-grained sandstone	97	73
K87-01	K87	3763.77	P_1f	Tuffaceous glutenite	90	59
817-02	817	3551.9		Pebbly medium- and fine-grained sandstone	98	79
B25-01	B25	3126.7		Medium- and coarse-grained sandstone	97	78
JL17-03	JL17	3786.2		Fine-grained sandstone	98	82
JL49-02	JL49	4569.6		Silty fine-grained sandstone	96	79
JL17-04	JL17	4622.1	P_1j	Pebbly medium- and fine-grained sandstone	99	74
G15-04	G15	4197.3		Medium- and coarse-grained sandstone	98	85

3.2. Detrital Zircon Dating

The separation and selection of zircons, the preparation of sample targets, the collection of cathodoluminescence (CL) images, and laser ablation inductively coupled plasma mass spectrometry (LA-ICP-MS) U-Pb dating of zircons were performed at the State Key Laboratory of Continental Dynamics of Northwest University. A detailed description of the method is presented in Appendix A. The detailed test results are shown in the supplementary Table S1.

The probability density plots (PDPs) and the pie chart of age distribution were created with detritalPy software [74]. The data from U–Pb dating of detrital zircons were analyzed using multi-dimensional scaling (MDS) to simplify the research subjects from multi-dimensional space to low-dimensional space for positioning, analysis, and classification. This method can measure the similarity between samples while preserving the original relationships among samples. Similar samples are more likely to belong to the same provenance system. The MDS diagrams were also plotted using detritalPy.

4. Results

4.1. Petrology

All samples in this study are compositionally and texturally immature to submature with lithic-rich (mean about Q13%, F22%, L65%), derived from a subset of thin sections collected from the cores. Representative samples are mainly fine- to coarse-grained lithic sandstones with grain sizes ranging from 0.1–1.5 mm (Figure 4). Most of the debris grains are subrounded to subangular, with poor to medium sorting. Some of the grain surfaces are degraded due to alteration. The quartz surfaces are cleaner and lack alteration. The lithic clasts are principally intermediate-felsic and intermediate-mafic volcanic clasts such as tuff, basalt, andesite, trachyte, rhyolite, gabbro, diabase, and so on. Sedimentary lithic clasts are subordinate including chert, mudstone, siltstone, and sandstone. The sandstone petrology is attesting to a dominantly volcanic provenance. Predominant euhedral detrital zircons in these samples and the presence of abundant lithic clasts in sandstones with low compositional and textural maturity imply proximal source areas.

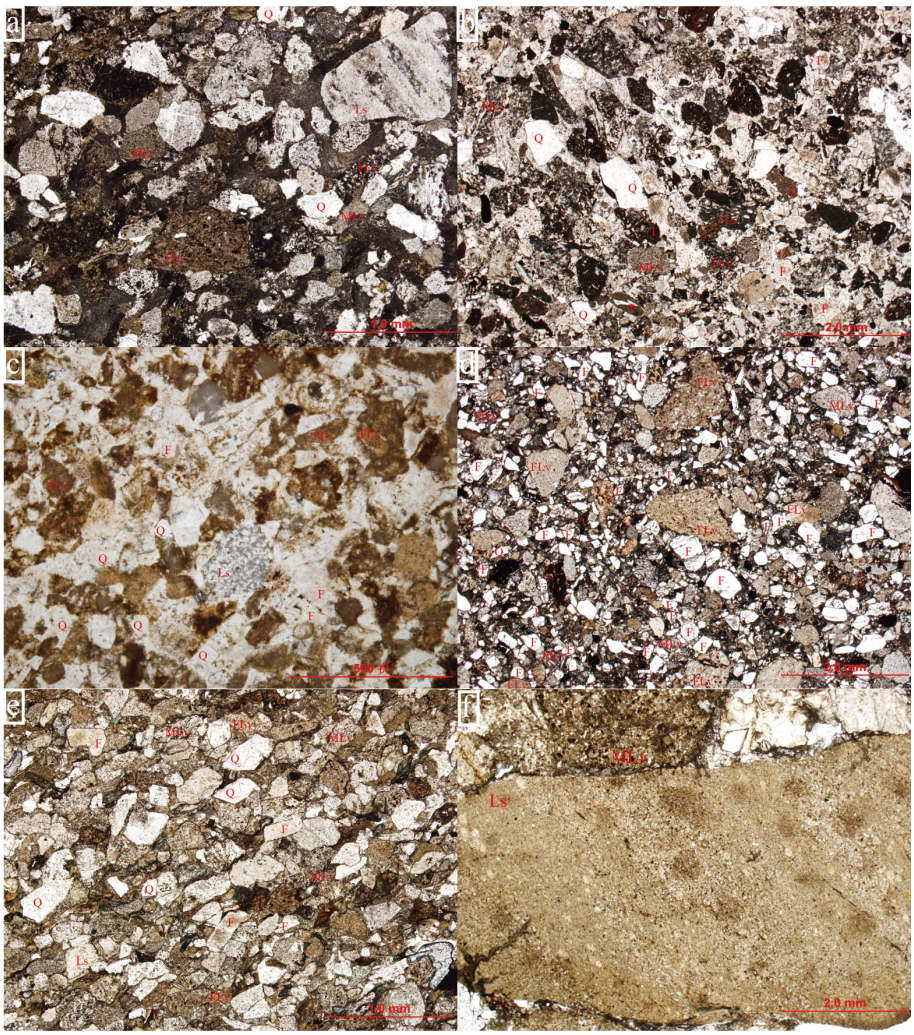

Figure 4. Representative photomicrographs of textures and minerals of the lithic clasts and detrital grains under plane-polarized light. The sandstone from the (**a**) Jiamuhe Formation (Sample ID: G15-04, sandstone clastic component: Q16%, F10%, L74%), (**b**) Fengcheng Formation (Sample ID: B25-01, Q11%, F22%, L67%), (**c**) Xiazijie Formation (Sample ID: 817-01, Q22%, F28%, L50%), (**d**) Lower Wuerhe Formation (Sample ID: MH012-2, Q6%, F29%, L65%) and (**e**) Upper Wuerhe Formation (Sample ID: JT1-2, Q9%, F21%, L70%). (**f**) The conglomerate with the pebbles of sedimentary and volcanic rocks from the Lower Wuerhe Formation (Sample ID: C73). Abbreviations of minerals: F, feldspar; FLv, felsic volcanic clasts; Ls, sedimentary lithic fragment; MLv, mafic volcanic clasts; Q, quartz; T, tuff.

4.2. Detrital Zircon Morphology and Element Geochemistry

Under the microscope, most detrital zircons are euhedral granular, and few are subhedral. The grains were mostly granular, subangular-columnar, or irregular. A few grains were elongated columnar or elliptical. Some zircon grains had rough surfaces and contained black inclusions. Some zircons were broken or had surface pits and cracks, with marginal erosions. The aspect ratios of zircon grains ranged from 1.0 to 3.0 and were mostly between 1.2 and 2.5. The crystal sizes ranged from ~50 μm to 250 μm, most of which were between 60 μm to 200 μm. Most of the zircon grains were moderate to well-sorted, with poor polish. Young zircon grains were almost angular to subangular, with no obvious signs of transport, indicating their spatial proximity to the provenance. Some older zircon grains were subangular to subcircular, indicating that they had undergone considerable transport and abrasion.

The U and Th contents and Th/U ratios are related to the genesis of zircons. Generally, magmatic zircons have high Th/U ratios (>0.4), and metamorphic zircons have low Th/U ratios (<0.1) [75]. In the samples collected in this study, zircons exhibited Th/U ratios >0.4 (Figure 5a). Besides, the detrital zircons were tested for rare earth element (REE) contents. The REE data is shown in the supplementary Table S3. ∑REE varies greatly, ranging from 64.981×10^{-6} to 26159.412×10^{-6}. The contents of light rare earth element (LREE) and heavy rare earth element (HREE) are 1.676×10^{-6}–17235.793×10^{-6} and 63.041×10^{-6}–8923.619×10^{-6} respectively. LREE/HREE value is between 0.005 and 2.658. It can be seen that the contents of REE have changed significantly. Chondrite-normalized REE plots were drawn for typical samples from five formations (Figure 5b). Most zircon grains have the characteristics of typical magmatic origin, that is, with obvious depletion of LREE and enrichment of HREE [76,77]. In addition, the majority of magmatic origin zircon grains exhibit obvious positive Ce anomaly and negative Eu anomaly in their REE patterns [78]. The corresponding Ce/Ce* and Eu/Eu* ratios are 0.815–667.556 (average: 35.674) and 0.0005–1.161 (average: 0.251) respectively. As well, detrital zircons show good crystal morphology and clear oscillatory zoning, as is the case of magmatic zircons (Figure 6). A small number of zircons exhibit typical sector zoning (e.g., sample MH012-2). Through comprehensive analysis of CL images, Th/U ratio, and REE data, the results indicated that all zircon grains were of magmatic origin.

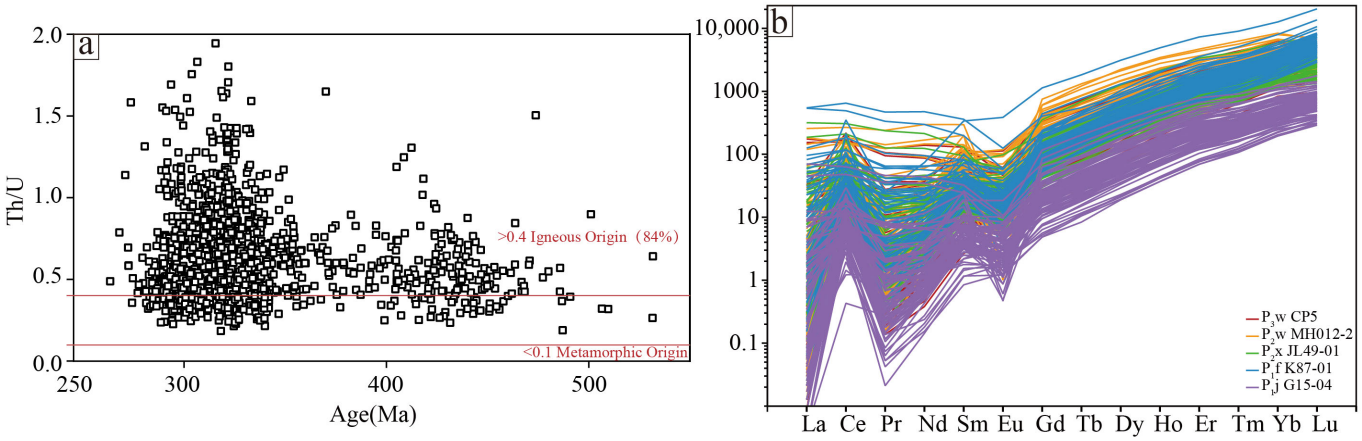

Figure 5. (**a**) The plot of Th/U ratios versus zircon U–Pb ages of detrital zircons from detrital samples in Permian deposits from the Mahu-Zhongguai area, northwestern Junggar Basin. (**b**) The chondrite-normalized REE patterns for zircons of magmatic origin for typical Permian samples from the Mahu-Zhongguai area, northwestern Junggar Basin.The values of chondrite are from [79].

4.3. Characteristics of U-Pb Ages of Detrital Zircons

The characteristics of U-Pb ages of detrital zircons from the collected Permian samples (Table 2, Figure 6) are described according to the stratigraphy as follows:

Table 2. Characteristics of the U-Pb ages of detrital zircons in the Mahu-Zhongguai area on the northwestern margin of the Junggar Basin.

Sample ID	Formation	Age range (Ma)	Dominant peak (Ma)	Main age range (Ma)	Secondary peak (Ma)	U-Pb age composition (%) Permian (299–252 Ma), Pennsylvanian (323–299 Ma), Mississippian (359–323 Ma)
MH012-01	P_3w	283–421	321		/	6, 90, 3
B252-4		296–464	318	320–323	420, 430	1, 43, 21
JL43		275–480	292, 310, 326	316–319	347, 405, 427	25, 31, 25
JT1-2		272–486	299, 311, 320	291–327	274, 340, 371, 388, 404, 424, 454	17, 41, 13
CP5		306–467	324, 333	296–322	406, 434, 465	0, 23, 59
SP1-2		277–454	293	319–348	280, 311, 323, 375, 395, 422	21, 29, 7
X6-2	P_2w	294–474	327	295–319	420	3, 31, 51
M19		271–446	326	312–335	272, 397, 440	8, 28, 48
M224		291–427	313	298–341	/	13, 49, 34
BW10-2		285–393	299	291–340	/	33, 56, 9
M009		286–426	297	290–326	/	41, 47, 11
M607		273–326	294	290–310	/	68, 30, 2
MZ7		274–348	294	287–307	/	78, 18, 4
MH012-2		286–421	302	286–305	/	34, 58, 5
JW27-12		305–468	322	289–316	359, 426, 444	0, 51, 25
JL17-01		297–451	321	319–323	306	1, 84, 8
G114-04		264–468	310, 322	318–324	266, 353, 371, 415, 436, 452	12, 30, 24
C73		288–467	311	295–325	337, 425, 465	15, 51, 21
JL49-01	P_2x	283–422	322	301–319	363	1, 59, 33
K87-01	P_1f	309–486	325	320–339	/	0, 15, 78
817-02		295–487	315	323–326	/	1, 77, 6
B25-01		320–446	322	313–318	351	0, 69, 23
JL17-03		298–458	326	320–332	299, 442	2, 13, 72
JL49-02		285–443	321	320–330	/	4, 73, 15
JL17-04	P_1j	297–348	314	311–323	/	3, 85, 8
G15-04		273–491	325	311–318	351, 441	5, 14, 59

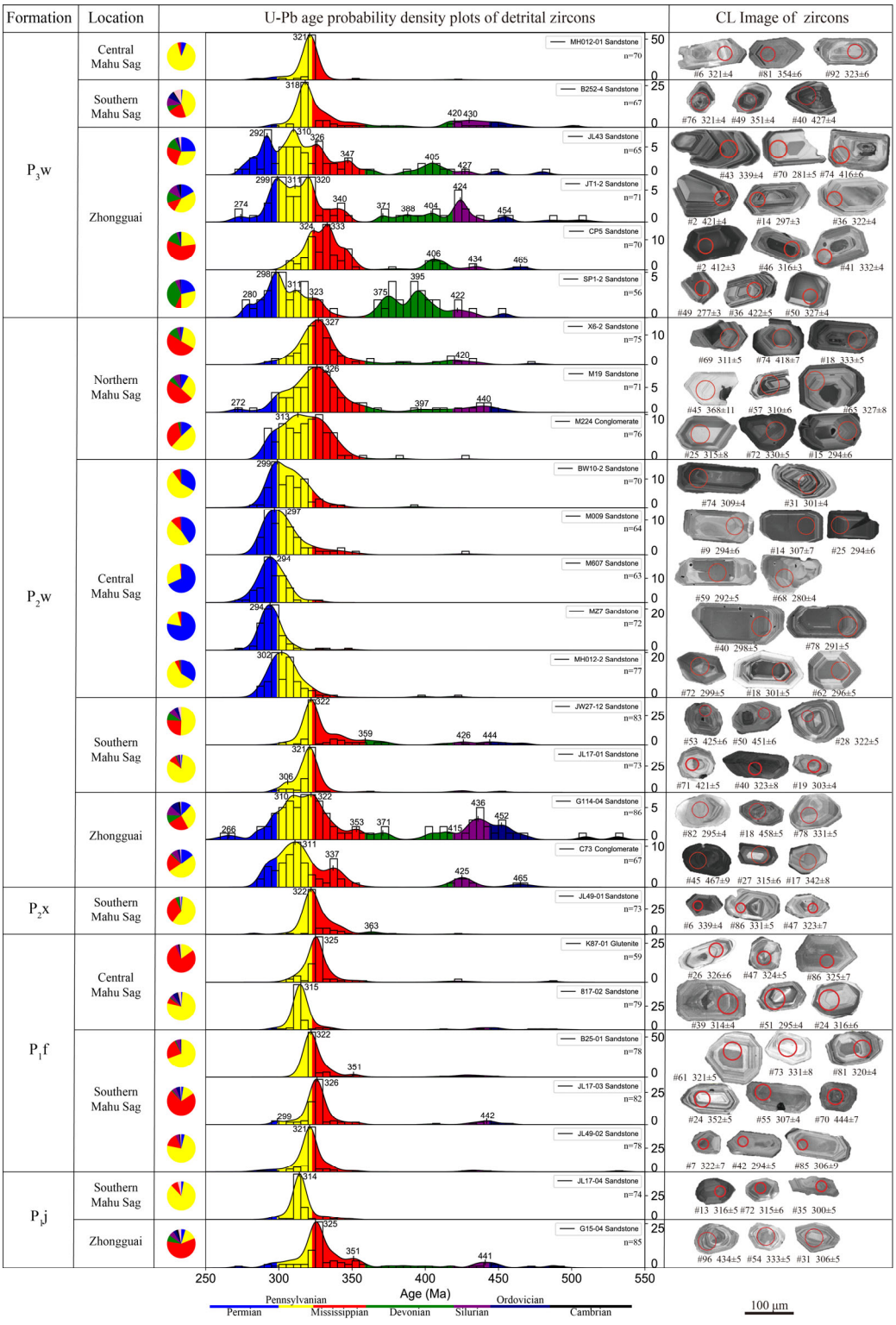

Figure 6. U-Pb age probability density plots of Permian detrital zircons from detrital samples in the Mahu-Zhongguai area, northwestern Junggar Basin. The age distribution is shown by a pie chart on the left for each sample. The cathodoluminescence images of some detrital zircon samples are shown in the rightmost column. The locations and details of detrital zircon samples are shown in Figure 1 and listed in Table 1.

Only two samples were collected from the Jiamuhe Formation (P1j): The zircon age of sample JL17-04 taken from the southern Mahu Sag (SMS) showed a sharp unimodal distribution concentrated in the Late Carboniferous, with a peak value of 314 Ma. The

zircon age of sample G15-04 collected from the ZU spanned a long period mainly from the Early Permian to the Early Ordovician, with the dominant peak at 325 Ma and the secondary peaks at 351 Ma and 441 Ma.

The five samples from the Fengcheng Formation (P1f) were all taken from the Mahu Sag. Their zircon ages were similar in distribution, range, and general characteristics. Specifically, their ages were concentrated in the Carboniferous, with a sharp peak between 315 Ma and 326 Ma. Compared with other samples, JL17-03 exhibited a broad age distribution and secondary peaks at 299 Ma and 442 Ma.

The only sample from the Xiazijie Formation (P2x), JL49-01, was taken from the SMS. The zircon ages were concentrated in the Carboniferous, with a dominant peak of 322 Ma and a secondary peak of 363 Ma.

A large number of samples were collected from the Lower Wuerhe Formation (P2w), covering the entire study area. These samples were roughly classified into three groups according to zircon age characteristics. The first group included the five samples collected from the central Mahu Sag (CMS) with similar zircon age characteristics, namely, a unimodal distribution concentrated between the Early Permian and the Late Carboniferous with a broad and gentle peak between 294 Ma and 302 Ma. The second group included samples JW27-12 and JL17-01 collected from the SMS and samples X6-2, M19, and M224 collected from the NMS, with a dominant peak between 313 Ma and 327 Ma and a small number of Devonian-Ordovician zircon grains. The third group included the two samples G114-04 and C73 taken from the ZU, with zircon ages ranging from the Early Permian to the Late Devonian and between the Early Devonian and Late Ordovician, a dominant peak at 310–322 Ma, and multiple secondary peaks.

The samples from the Upper Wuerhe Formation (P3w) were divided into two groups according to zircon age. The first group included sample MH012-01 collected from the CMS, which had a unimodal zircon age distribution with a dominant peak at 321 Ma, indicating that the provenance was relatively simple. The second group included the five samples collected from the SMS and the ZU, which exhibited complex multimodal zircon age distributions with a broad age span mainly ranging between the Late Permian and the Early Carboniferous and between the Late Devonian and Middle Ordovician.

According to the stratigraphic sequence, the samples from the Jiamuhe Formation, Fengcheng Formation, and Xiazijie Formation were relatively similar in zircon age distribution and characterized by a narrow peak in the Carboniferous, indicating a relatively simple provenance. The samples from the Lower Wuerhe Formation and the Upper Wuerhe Formation showed relatively wide zircon age ranges and variable peak values, reflecting the growing complexity of the provenance. In addition, the samples from the Lower Wuerhe Formation and the Upper Wuerhe Formation contained greater numbers of Permian detrital zircons, reflecting the possible presence of deposits of proximal Permian recycled sediment. From the sample distribution, the proportion of Early Paleozoic zircons gradually increased from the CMS southward to the ZU.

5. Discussion

5.1. Age Distribution Characteristics and Parent Rock Properties of the Potential Source Area

Clarifying the stratum outcrops in the potential provenances and the geochronological framework of magmatic rocks is one of the basic tasks for provenance analysis. This paper analyzed the published isotope age data for 643 magmatic rock samples from different regions of the West Junggar (Figure 7) and divided the study area into five units (the ZhSA in the NWJ, the BCA, the CWJ, the SWJ, and the island arc on the northwestern margin of the Junggar Basin) for statistical analysis as described in section 2.

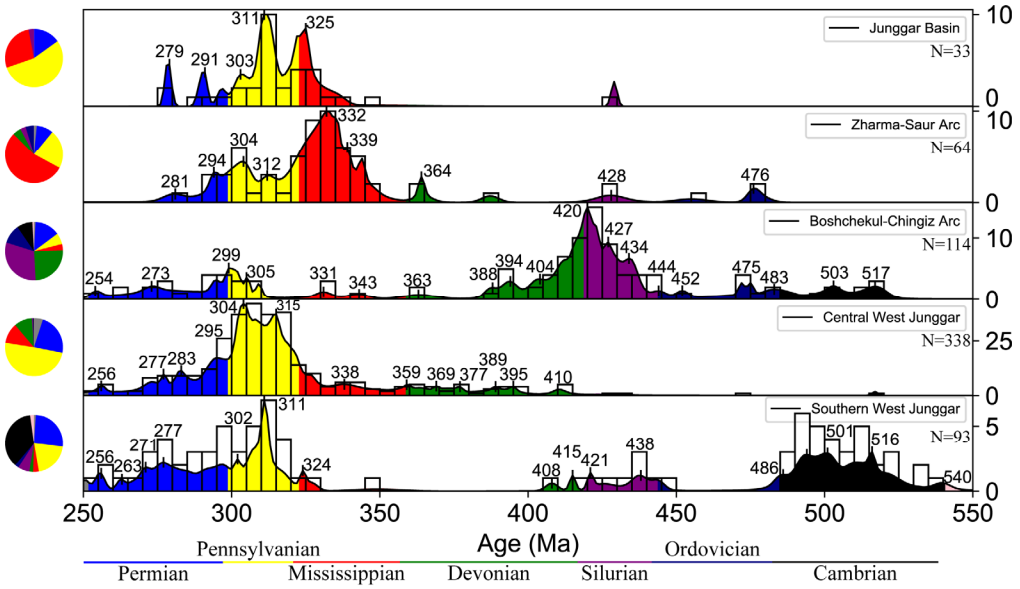

Figure 7. Zircon age distributions of magmatic and metamorphic rocks in northern West Junggar (NWJ), including the Zharma-Saur arc and Boshchekul-Chingiz arc, central West Junggar (CWJ), southern West Junggar (SWJ), and the Junggar Basin, shown as histograms, probability density plots, and pie charts. Data from Xu et al. [31], Chen et al. [40], Yang et al. [45], Li et al. [80], Li et al. [81], Jian et al. [82], Han et al. [83], Zhou et al. [84], Geng et al. [85], Chen et al. [86], Feng et al. [87,88], Shang et al. [89], Tang et al. [90], Yang et al. [91], Tian et al. [92], Xiang et al. [93], Zhang et al. [94], Jin et al. [95], Chen et al. [96], Tang et al. [97], Yin et al. [98], Yin et al. [99], Duan et al. [100].

The results of the analysis show that the age distributions of the five potential provenances are significantly different (Figure 7). The magmatic activity in the NWJ was obviously divided into the Late Paleozoic ZhSA in the north and the Early Paleozoic BCA in the south. The zircon ages of the ZhSA were mainly from the Carboniferous. The zircon ages of the BCA were mainly distributed between the Late Devonian and the Silurian with sporadic representation from the Carboniferous, Ordovician, and Cambrian. The stratigraphic ages of the CWJ were concentrated in the Late Carboniferous and Permian, and additionally included material aged from the Early Carboniferous and Devonian but not the Early Paleozoic. Compared with the NWJ and CWJ, the ages of samples from the SWJ were widely distributed in the Early Paleozoic but did not include material from the Early Carboniferous, Devonian, or Ordovician. The zircon ages in the interior of the Junggar Basin showed a continuous distribution from the Permian to the Carboniferous.

The intense Paleozoic volcanic activity in the West Junggar formed strata dominated by volcanic rocks and volcanic clastic rocks. The NWJ showed widely developed Devonian-Silurian (394–434 Ma) mafic and felsic volcanic rocks [98,101] and sporadic outcrops of Early Carboniferous (325–343 Ma) intermediate-mafic volcanic rocks [102–104] and Permian volcanic rocks [105,106]. Carboniferous-Devonian intermediate-mafic volcanic rocks were widely developed in the CWJ and SWJ [107,108]. In addition, the SWJ showed outcrops of Middle Ordovician intermediate-mafic volcanic lava [49].

Mafic and felsic intrusive rocks from the Early Permian to the Late Ordovician have been discovered in the WJ [48,84,109,110]. The ZhSA mainly showed outcrops of Early Carboniferous (321–346 Ma) intermediate-felsic rocks but also showed a small number of outcrops of Early Permian-Late Carboniferous (283–304 Ma) intermediate-felsic rocks [40,111]. The BCA mainly showed outcrops of Late Devonian-Late Silurian (380–445 Ma) mafic, intermediate-felsic rocks [111,112]. The CWJ and SWJ showed a wide range of outcrops of Middle Permian-Late Carboniferous (287–322 Ma) intermediate-felsic rocks [40,83]. The SWJ had very few mafic rocks emplaced between the Middle Silurian and the Late Cambrian (425–501 Ma) [31,49].

Ophiolitic mélange belts from the Late Paleozoic to the Neoproterozoic were developed in the WJ [109,110]. The ophiolitic mélange belts in the NWJ were mainly formed in the Early Ordovician (472–478 Ma) [35,82,113], and a few were formed in the Middle Cambrian (517–519 Ma) [114,115]. The ophiolitic mélanges exposed in the CWJ were obviously younger and were mostly formed from the Late Carboniferous to the Early Silurian (335–435 Ma) [116,117]. Late Silurian-Late Neoproterozoic (435–572 Ma) ophiolitic mélanges have been discovered in the SWJ [118].

It Is worth noting that there are multiple Early Permian-Carboniferous island arcs in the Junggar Basin [27,119] For example, Early Carboniferous island-arc volcanic rocks (mainly including andesite, basalt, and rhyolite) were developed under the Meso-Cenozoic strata of the ZU and the Kebai fault on the northwestern margin [120,121], and their ages were concentrated between 290 Ma and 325 Ma, corresponding to the subduction period of the island arcs in the WJ.

5.2. Comparison of the Age Distribution Characteristics of the Depositional Area and the Source Area

In general, sediments with the same provenance are similar in detrital zircon age distribution, while sediments differing in provenance with strata containing rocks of obviously different ages show different distributions of detrital zircon age. In this paper, the detrital zircon ages of the rocks in outcrop on the northwestern margin of the Junggar Basin were compared with the detrital zircon ages of the Permian rocks in the basin to comprehensively analyze the information on the Permian provenances at the northwestern margin and their evolution.

5.2.1. Jiamuhe Formation (P1j)

The detrital zircon ages of sample JL17-04 from the SMS were mostly from the Early Carboniferous (310–320 Ma) (Figure 6), which is consistent with the emplacement ages of the Carboniferous volcanic rocks and granites currently outcropping in the CWJ and the ZhSA (Figure 7). No Devonian or Silurian-Ordovician detrital zircons have been discovered which may relate to the synchronous volcanic activities in SWJ and the BCA, indicating that these were not the provenances. Li et al. Li, et al. [119],[122] suggested that the ZhSA, the BCA, and the Junggar terrane amalgamated between the Early Devonian and the Early Carboniferous, so the detrital material of the ZhSA could not be transported across the BCA to the Junggar Basin during the depositional period of the Jiamuhe Formation [123]. Therefore, the ZhSA was likely not a provenance. The poor roundness and the angular to subangular shapes of detrital zircon grains (Figure 6) indicated that the SMS was mainly affected by the proximal CWJ in the north.

The detrital zircon ages of sample G15-04 from the ZU ranged continuously from the Early Permian to the Early Ordovician (273–491 Ma), with one dominant peak and multiple secondary peaks (peaks values at 325, 351, and 441 Ma from high to low contents), indicating that G15-04, which had multiple provenances, showed higher provenance complexity than JL17-04. Overall, the zircon age distribution of ZU between the Early Permian and Early Carboniferous (294–358 Ma) is most similar to that of the CWJ, which indicated that the zircons were mainly from proximal Carboniferous magmatic rocks in the CWJ. Considering that the Silurian-Ordovician age range is missing in the CWJ and that the sample had a peak age of 441 Ma, it is speculated that the Zhongguai area might have not only the dominant provenance in the CWJ but also secondary provenances in SWJ and the BCA. The adjacent Ordovician-Silurian series of the SWJ southwest of G15-04 was most likely to contribute to the provenance because of the absence of Silurian zircon in sample JL17-04, which was north of sample G15-04, and the moderate roundness of zircons (Figure 6). Hence, the source of sample G15-04 from the Jiamuhe Formation was mainly from the proximal CWJ and partially from the distal SWJ.

5.2.2. Fengcheng Formation (P1f)

Samples K87-01 and 817-02 of the Fengcheng Formation were taken from the CMS, and samples B25-01, JL17-03, and JL49-02 were taken from the SMS. The five samples showed relatively similar zircon age distributions, namely, unimodal distributions mainly concentrated in the Carboniferous (310–330 Ma) with a sharp peak, and the zircon grains were mostly euhedral (Figure 6). The results indicated that the Fengcheng Formation during the depositional period had a relatively simple and limited provenance, which is speculated to be a Carboniferous geological body in the proximal CWJ.

Compared with other samples, sample JL17-03 showed a wider age distribution, with secondary peaks at 299 Ma and 442 Ma. The age of 442 Ma only occurred in the Silurian series in the BCA and SWJ, and the provenance was more likely to be located in the northwest (Figure 6), which indicated that the BCA was more likely to be the provenance. Sample JL17-03 of the Fengcheng Formation from the same well, JL17, exhibited a wider range of zircon ages, which indicated that the provenance range was expanded. The zircon ages changed from a unimodal distribution to a multimodal distribution, indicating the presence of multiple provenances. The dominant peak changed from 314 Ma to 326 Ma, indicating that the provenance was likely to be older strata or rock bodies.

5.2.3. Xiazijie Formation (P2x)

Sample JL49-01 of the Xiazijie Formation was taken from the SMS. The zircon ages of JL49-01 were mostly concentrated between 320 Ma and 324 Ma, with a dominant peak and a small secondary peak (Figure 6), indicating that the source was relatively simple. Sample JL49-01 of the Xiazijie Formation and sample JL49-02 of the Fengcheng Formation were taken from the same well, JL49, and their age distribution characteristics were also similar. Hence, their sources showed a certain inheritance. In other words, the sediments mainly originated from the CWJ. However, sample JL49-01 also contained Devonian zircons (363 Ma), which may be derived from the Darbut ophiolitic mélange in the CWJ [124] or Upper Devonian rocks [46]. Therefore, the source of sample JL49-01 was mainly from the nearby CWJ in the northwest. It should be noted that only one sample of the Xiazijie Formation was analyzed here, so uncertainty maybe exist.

5.2.4. Lower Wuerhe Formation (P2w)

This paper focuses on the provenance analysis of the Lower Wuerhe Formation. Before comparing the age distribution of the depositional area with that of the provenance, the zircon-tourmaline-rutile (ZTR) index of the depositional area was briefly analyzed as a provenance indicator [125]. The detailed data table of the ZTR index is shown in the supplementary Table S2.

1. Planar distribution characteristics of the ZTR index of the depositional area

The ZTR index is often used to reflect the maturity and provenance direction of clastic rocks. It is the ratio of the total content of zircon, tourmaline, and rutile to the total content of transparent heavy minerals. Because of high mechanical and chemical stability, zircon, tourmaline, and rutile are concentrated as the compositional maturity of sandstones becomes progressively higher [126–128]. Thus, the variation trend of the ZTR index on the plane can indicate the transport direction of sediments and the location of the source area [129]. Higher values of the ZTR index generally indicate greater distances from the provenance, and vice versa [130]. By comparing the spatial variation in the ZTR values of 80 heavy minerals in the Lower Wuerhe Formation, it is observed that the ZTR values of the NMS mainly increased southwestward (Figure 8), indicating that there might be a provenance in the northeast at this time. The ZTR values of the CMS did not show a clear trend. The ZTR values of the SMS and ZU increased eastward and southeastward, respectively, indicating that the provenance in the west or northwest at this time supplied the detrital material into the basin. Given that the ZTR index has certain limitations in reflecting the provenance direction, other evidence is needed to determine the Permian provenances.

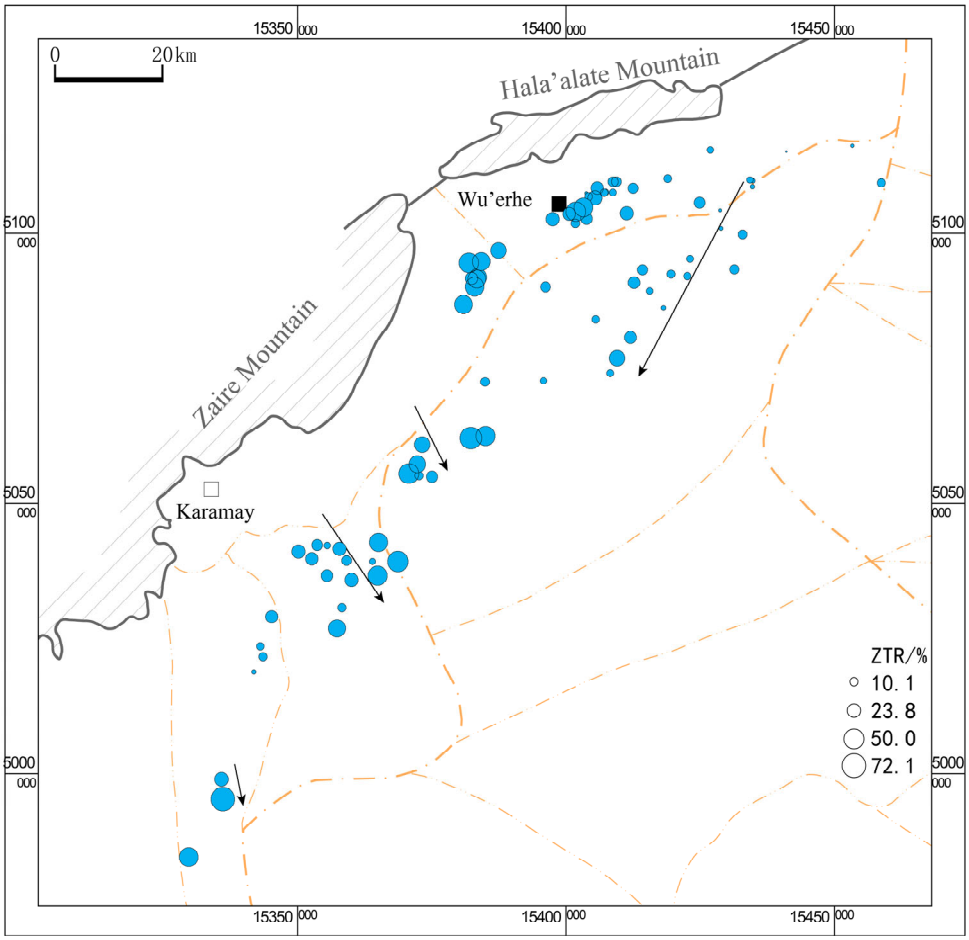

Figure 8. Spatial distribution of the zircon-tourmaline-rutile (ZTR) index of the Lower Wuerhe Formation in the Mahu-Zhongguai area

2. Age distribution characteristics

The samples from the Lower Wuerhe Formation were roughly divided into four groups according to the age characteristics and the locations of the sampling sites, reflecting the possibility that adjacent wells of the depositional areas with similar patterns might be in the same provenance system (Figure 6, Figure 9):

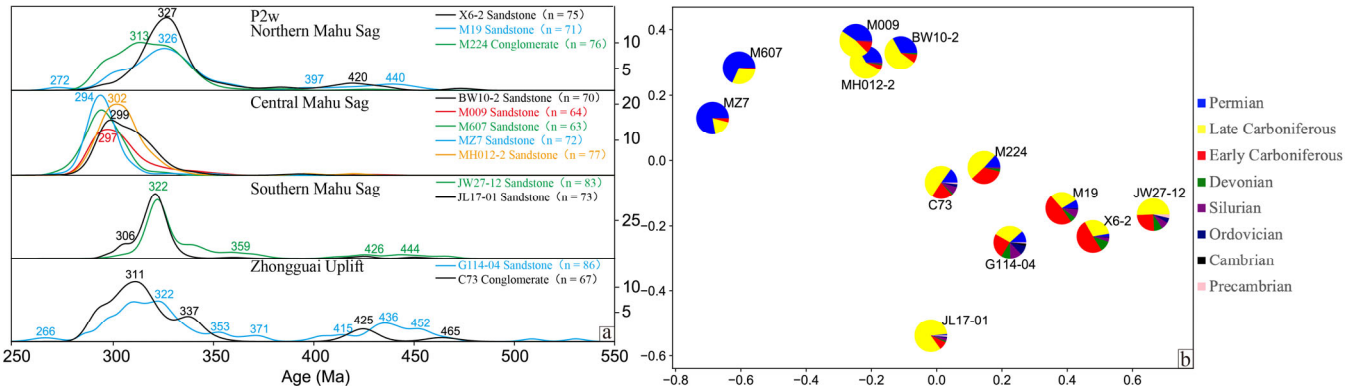

Figure 9. (**a**) Distributions of U-Pb ages of detrital zircons in the Lower Wuerhe Formation in the Mahu-Zhongguai area, northwestern Junggar Basin. (**b**) Multidimensional scaling diagram. The samples were classified according to the similarity of age distribution characteristics and geographical location. The multi-dimensional scaling diagrams can measure the similarity of multiple samples in different locations but in the same period. The locations and details of detrital zircon samples are shown in Figure 1 and listed in Table 1.

The first group of samples, X6-2, M19, and M224, were taken from the NMS. The zircon ages ranged widely and exhibited a broad and gentle dominant peak and multiple secondary peaks, indicating high provenance complexity and multiple provenances. The zircon ages were mainly between 290 Ma and 345 Ma. The material may originate mainly from the Early Permian-Late Carboniferous magmatic rocks developed in CWJ and the ZhSA and might be partially from the BCA. This group of samples contained some Devonian-Late Ordovician detrital zircons, indicating that the sediments were partly from the Devonian-Silurian volcanic rocks and the Early Devonian-Late Silurian intrusions in the BCA. The ZTR index analysis indicated that the provenance direction was from north to south (Figure 8). In general, the main provenances of the NMS were CWJ and the ZhSA, and a small amount of older terrigenous detrital material is derived from the BCA.

The second group of samples, BW10-2, M009, M607, MZ7, and MH012-2, were taken from the CMS. Their detrital zircon age distribution was unimodal with a broad and gentle peak, indicating that the provenance was relatively limited. The abundance of Early Permian-Early Carboniferous zircons in the CMS was significantly higher than those in other depositional areas of the same period, and this pattern may be closely related to the extensively developed Early Permian granite and diorite intrusions as well as the gabbro and diabase dikes in the Zaire and Hala'alate Mountains in CWJ [83,85,87,113,131,132]. Therefore, it is speculated that the detrital material was mainly from CWJ. The lack of zircon ages from the Silurian to the Devonian indicated that the provenance system did not extend northward to the BCA.

The third group of samples, JW27-12 and JL17-01, were taken from the SMS. The age spectrum of detrital zircons was roughly similar to those of the Jiamuhe Formation and Fengcheng Formation in Well JL17 mentioned before (the detrital zircon ages were mainly from the Carboniferous), which indicated that the provenance had a certain inheritance, principally from the Carboniferous magmatic rocks in CWJ. The zircon age distribution range of sample JW27-12 was wider than that of JL17-01, with one dominant peak and multiple secondary peaks, indicating that JW27-12 was a mixed-source deposit. The 426 Ma zircons might derive from the Darbut ophiolite belt [133] or the Silurian intermediate-felsic magmatic rocks in the Xiemisitai Mountains [134,135]. The 444 Ma zircons might originate from the Sugensala rocks in the Xiemisitai Mountains [136] or the Hongguleleng ophiolitic mélange belt [137]. The provenance direction was determined to be from north to south based on ZTR analysis (Figure 8). It is speculated that the source of the SMS was mainly provided by the proximal CWJ, while a small portion was provided by the distal NWJ.

The fourth group of samples, G114-04 and C73, were taken from the ZU. Their detrital zircon age spectrum was broader than that of the adjacent SMS during the same period, with zircon ages mainly distributed in two discontinuous intervals: 266–371 Ma and 415-452 Ma. Early Permian-Late Devonian magmatic rocks are widely distributed in the CWJ, SWJ, and ZhSA [31]. Considering the ZTR-indicated provenance direction from west to east (Figure 8) and the poor roundness of most zircons, the proximal CWJ and SWJ were more likely to be the potential provenances. This group of samples contained more Early Devonian–Early Silurian zircons than the samples from the SMS did, and the zircons of these ages might mainly derive from SWJ, including the Mayile ophiolite belt [138], the Tangbale ophiolite belt [28], and the intrusive rocks in the Mayile Mountains [31], which indicated that the ZU was more affected by the sediment supply from SWJ. It is worth noting that sample G114-04 contained ~10% of the Ordovician zircons, but there is no record of volcanic activity from the Middle-Late Ordovician throughout West Junggar (Figure 7) [28,52,139]. The Ordovician series was only developed in SWJ, with a large quantity of Middle-Late Ordovician magmatic detrital zircons in the sedimentary strata [31,109,140]. This finding may imply that the Ordovician magmatic zircons in the area adjacent to SWJ were transported to SWJ to form detrital zircons. The 467 Ma zircons in sample C73 were subrounded (Figure 6), indicating that the detrital zircons were transported for a certain distance. Therefore, the Ordovician detrital zircons likely originated

from the deposits of the Ordovician recycled sedimentary rocks from SWJ. In summary, the terrigenous detrital sediment in the ZU derived from the mixed source supply from CWJ and SWJ; the sediment supply from SWJ was significantly higher than that during the depositional period of the Jiamuhe Formation.

5.2.5. Upper Wuerhe Formation (P3w)

The samples from the Upper Wuerhe Formation were roughly classified into three groups (Figure 6, Figure 10a):

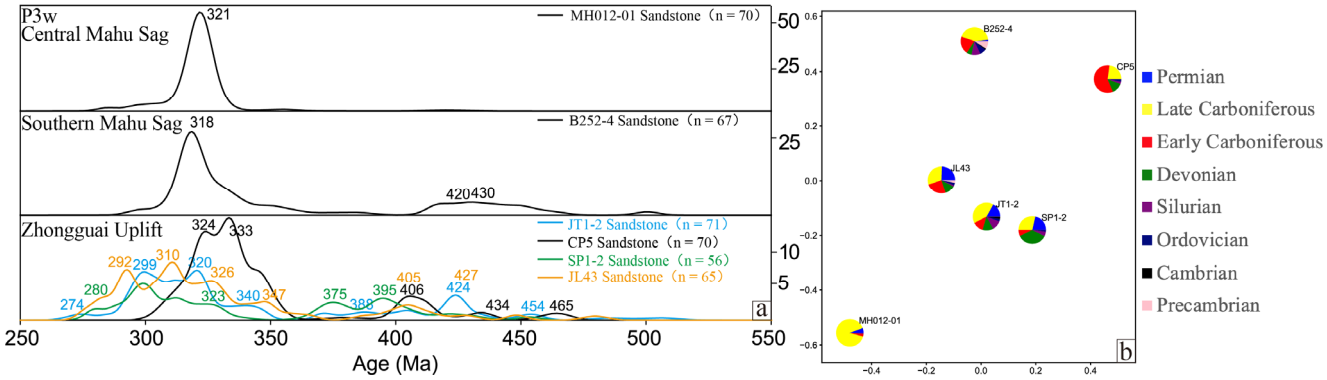

Figure 10. (**a**) Diagram of U-Pb detrital zircon age distribution in the Upper Wuerhe Formation in the Mahu-Zhongguai area, northwestern Junggar Basin. (**b**) Multidimensional scaling diagram. The samples were grouped according to the similarity in age distribution characteristics and geographical location. The multi-dimensional scaling diagram shows the similarity of multiple samples in different locations but in the same period. The locations and details of detrital zircon samples are shown in Figure 1 and listed in Table 1.

The first group included sample MH012-01. The sample was taken from the CMS. Its age spectrum was unimodal with a sharp peak, indicating that its provenance was simple and limited. The detrital zircon ages were concentrated in the early stage of the Late Carboniferous (321 Ma), and Carboniferous magmatic rocks were widely distributed in WJ, forming potential provenances. The provenance direction from north to south [68] and the angular zircons indicated that the adjacent CWJ provided the source. This sample did not show the Devonian ages associated with the ophiolitic mélange or the Ordovician-Devonian ages, indicating that the provenance system did not extend southwestward to SWJ, and the basin did not reach NWJ. Therefore, the material in the CMS was mainly sourced from CWJ.

The second group included sample B252-4, which was taken from the SMS. Its detrital zircon was mainly aged from the Carboniferous, while the Carboniferous series was distributed throughout the potential provenances. A small portion of zircon from the sample was aged from the Early Devonian-Late Ordovician (395–430 Ma), and the magmatic zircons of this age range were only developed in SWJ and the BCA and might have provided detrital material. The zircon cathodoluminescence images (Figure 6) show that the 427 Ma zircons in sample B252-4 were subrounded to subangular, suggesting that they underwent long-distance transport. According to the contour map of the sand-to-formation ratio, the source was transported from the northwest [68]. Therefore, it is speculated that the Early Permian-Early Carboniferous zircons might originate from the adjacent CWJ, while the Devonian-Ordovician zircons were mainly from the distant BCA. In summary, the source of the SMS was dominantly from the CWJ, a nearby provenance, and a small portion of the source of the SMS was derived from the NWJ, a distant provenance.

The third group included samples JL43, JT1-2, CP5, and SP1-2, which were collected from the ZU and its adjacent areas. These samples were extremely similar in age characteristics, which indicated that they were affected by the same provenance system. Their

zircon age spectra were multimodal, with a continuous distribution from the Early Permian to Middle Silurian (270–430 Ma) and a small portion of Late Ordovician-Middle Ordovician ages. The Devonian-Cambrian magmatic rocks were mainly found in the BCA and were also exposed in SWJ. The Devonian series was also present in CWJ, and Permian-Carboniferous magmatic rocks were distributed throughout WJ. It can be speculated that the terrigenous detrital material mainly originated from CWJ and SWJ based on the provenance direction from west to east [68]. It is worth noting that the samples contained ~25% Early Permian (270–300 Ma) zircons, which may be related to the Permian felsic intrusions and mafic dikes widely developed in CWJ [32,50,53,80,81] based on the distributional characteristics of magmatic rocks in WJ. This finding is consistent with the widely observed granite gravel and debris components in the drilling cores of the Upper Wuerhe Formation in the Mahu-Zhongguai area [10]. In summary, the main provenances of the ZU were CWJ and SWJ. The ZU was different from the adjacent SMS in that it also received the sediment supply from SWJ. In summary, CWJ was still the main provenance of the ZU, but the sediment supply from SWJ was also important, and the sediment supply was higher than that during the depositional period of the Lower Wuerhe Formation.

It should be noted that the Permian series in the thrust belt and the island arc in the same period in the basin might also have provided the source. The thrust belt on the northwestern margin was active in the Early Carboniferous, Middle-Late Permian, and Late Triassic [8,29]. The rapid denudation of the hanging wall with fault development and the flexural subsidence and the massive sedimentary filling of the footwall resulted in the recycling of sediments [9,141,142]. At the same time, the Late Paleozoic island arcs developed in the basin [27,119,143] and exhibited a relatively strong correlation with the Permian-Carboniferous detrital zircons [55–57,120,121,144]. It is speculated that the island arcs in the interior of the basin may also have provided detrital material. However, since these provenances (the island arcs in the interior of the basin) could not be distinguished from other potential provenances outside the basin, this paper does not discuss them in detail.

5.3. Source-to-Sink System Division and Provenance System Evolution

In this paper, from the perspective of the source-to-sink system and tectonic-sedimentary response, the detrital sedimentary records of the northwestern margin of the Junggar Basin since the Permian were used to analyze the sedimentary response of Permian tectonic evolution and explore the indicator significance of the detrital zircon age distribution characteristics of the depositional area for the development of the provenances and the evolution of the basin-range pattern in the orogenic belt of WJ.

5.3.1. Source-to-Sink System Division

The detrital zircon age data have been logically interpreted to propose four source-to-sink systems from northeast to southwest based on the provenance analysis and variation in provenance characteristics across the Permian sedimentation (Figure 11): the source-to-sink system with CWJ and NWJ as the provenances and the NMS as the depositional area (i.e., the CWJ + NWJ→NMS system and hereafter termed NMS system), the source-to-sink system with CWJ as the provenance and the CMS as the depositional area (i.e., the CWJ→CMS system and hereafter termed CMS system), the source-to-sink system with CWJ and NWJ as the provenances and the SMS as the depositional area (i.e., the CWJ + NWJ→SMS system and hereafter termed SMS system), and the source-to-sink system with CWJ and SWJ as the provenances and the ZU as the depositional area (i.e., the CWJ + SWJ→ZU system and hereafter termed ZU system). The provenances varied among locations for the same period, while the source-to-sink system at the same location showed a certain inheritance among periods.

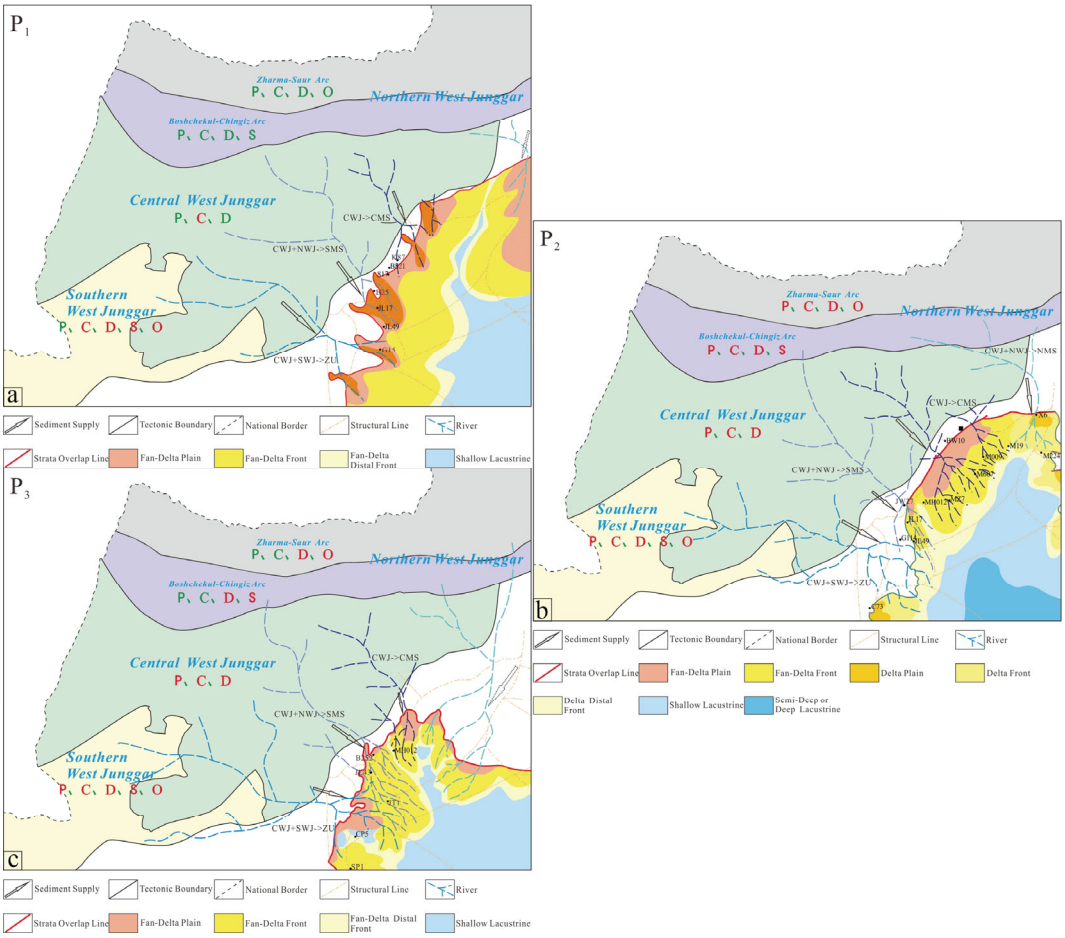

Figure 11. Schematic diagram of the distribution of the source-to-sink systems during the **(a)** Early Permian, **(b)** Middle Permian and **(c)** Late Permian in the Mahu-Zhongguai area, northwestern Junggar Basin. CWJ + NWJ→NMS: The source-to-sink system with central West Junggar (CWJ) and northern West Junggar (NWJ) as the main provenances and the northern Mahu Sag (NMS) as the depositional area. CWJ→CMS: The source-to-sink system with CWJ as the provenance and the central Mahu Sag (CMS) as the depositional area. CWJ + NWJ→SMS: The source-to-sink system with CWJ and NWJ as the main provenances and the southern Mahu Sag (SMS) as the depositional area. CWJ + SWJ→ZU: The source-to-sink system with CWJ and southern West Junggar (SWJ) as the provenances and the Zhongguai Uplift (ZU) as the depositional area. The green capital letters indicate the potential parent rock ages in each unit; the red capital letters indicate the possible stratigraphic age to provide the sediments in the area. The distribution map of sedimentary facies was prepared by the Xinjiang Oilfield Company. Note: The Upper Permian series in the NMS was eroded, and relevant data of the lower Permian series was lacking. Therefore, the CWJ + NWJ→NMS systems in the Early and Late Permian were all results speculated according to the inheritance of the source-to-sink systems and are represented by dashed lines in the figure.

1. Jiamuhe Formation

During the depositional period of the Jiamuhe Formation, the source-to-sink systems of the SMS and the ZU differed greatly (Figure 11a). The source of detritus in the SMS system was relatively simple, mainly the Early Carboniferous zircons from CWJ. The source of detritus in the ZU system was mainly the Carboniferous magmatic rocks in CWJ, with a small portion of mixed Silurian-Devonian supply from SWJ.

2. Fengcheng Formation

During the Fengcheng Formation's depositional period, the CMS system's provenance was relatively simple, mainly the Carboniferous series in CWJ. The SMS system was dominated by proximal Carboniferous detrital sediment supply from CWJ, and the presence of Silurian zircon marked the distal sediment supply from NWJ (Figure 11a).

In summary, three source-to-sink systems were developed in the Mahu-Zhongguai area during the Early Permian (Figure 11a). It should be noted that the NMS system was an inferred result based on the inheritance of the source-to-sink system due to the lack of NMS-related samples and data.

3. Xiazijie Formation

During the depositional period of the Xiazijie Formation, the source of the SMS system was relatively simple (Figure 11b) (mainly the proximal Carboniferous magmatic rocks in CWJ) and was inherited.

4. Lower Wuerhe Formation

During the depositional period of the Lower Wuerhe Formation (Figure 9), the Mahu-Zhongguai area was divided into four major source-to-sink systems, and the sediments were mainly from the adjacent mountain series in CWJ, such as the Zaire and Hala'alate Mountains (detailed in section 4.1, 4.2 and 5.2.4) (Figure 11b). The division of source-to-sink systems was the most complete due to a large number of samples in the study area and their relatively uniform distribution during the depositional period of this formation. Due to the difference in provenance during the depositional period, the source from the Zaire and Hala'alate Mountains in CWJ were deposited along different distributary channels. Among the four source-to-sink systems, the NMS system showed U-Pb zircon ages mainly from the Permian-Carboniferous period and had CWJ and NWJ as the provenances. The provenance range of this system extended more toward NWJ compared with those of the other three source-to-sink systems. The depositional system in the Mahu Sag was limited in distribution from the center of the lake basin to at most M19. The CMS system exhibited the simplest sources, most of which were Permian-Late Carboniferous zircons, from a limited provenance (mainly CWJ). This source-to-sink system was distributed widely in the depositional area and extended to the depositional center, to at least M009 northeastward, and to at least M012-2 southwestward, indicating that the provenance provided a relatively large supply of sediments. It is worth mentioning that the Darbut strike-slip fault zone extends from the mountain to the basin, and the channel formed between Zaire Mountain and Hala'alate Mountain may be an important channel for the supply of a large volume of sediments [145] and an important cause and the main area for the formation and development of the depositional system. The SMS system had a simple distribution of zircon ages, which were concentrated in the Carboniferous, with a small portion in the Silurian. The system had a mixed source supply, with most sediments from CWJ and a small portion from NWJ. This depositional system had a relatively limited distribution in the Mahu Sag and extended to at most JL17-01. The ZU system showed a broad multimodal distribution of zircon ages. The system was simultaneously affected by CWJ and SWJ, with the sediment supply from CWJ exceeding that from SWJ. The provenance system extended to SWJ.

It is worth noting that sample JL17-01 collected from the middle of the SMS system was not similar to sample G114-04 collected from the nearby ZU system or sample MH012-2 collected from the CMS system (Figure 9b). It can be speculated that the three samples belonged to different source-to-sink systems and that the source-to-sink systems were not mixed at the sampling sites. Similarly, sample M19 in the NMS system and sample M009 in the CMS system also differed significantly in U-Pb zircon age distribution characteristics, with no apparent similarity (Figure 9b), indicating that the two samples belonged to different source-to-sink systems and were not affected by source mixing.

5. Upper Wuerhe Formation

During the depositional period of the Upper Wuerhe Formation (Figure 10), the Mahu-Zhongguai area inherited the four source-to-sink systems of the Lower Wuerhe Formation (Figure 11c). The depositional system of the NMS system was denuded. The main source of the CMS system was CWJ. The SMS system had a mixed source supply,

with most sediments from CWJ and a small portion of sediments from NWJ. The ZU system was simultaneously affected by CWJ and SWJ, and the sediment supply from CWJ was slightly greater than that from SWJ. Compared with other source-to-sink systems in the same period, the ZU system was more affected by the material from SWJ.

It is worth noting that Zou et al. [68] classified samples JL43, JT1-2, and B252-4 into the same depositional system according to the sand-to-formation ratio contour map. The author believed that this depositional system had the largest scale during the depositional period of the Upper Wuerhe Formation. Due to the high content of lithic clasts with low compositional and textural maturity, the Upper Wuerhe Formation was characterized by closing to sediment source. Thus, the source of this system was mainly the adjacent Zaire Mountain in the north and secondarily the ZU in the west. However, the results of this study showed that sample JL43 was very similar to samples JT1-2 and SP1-2 but quite different from the adjacent sample B252-4 (Figure 10b). The results indicated that sample JL43 was mainly affected by the ZU system, with a certain sediment supply from the SMS system. It is further inferred that in samples collected from this depositional system, the sample (B252-4) that was closer to the provenance system was affected only by the SMS system. While the sample (JL43) that was farther from the provenance system received sediment supply simultaneously from the SMS and ZU systems since the sample was located between the two. Hence, it can be speculated that the depositional system was relatively complex, with the mixed sediment supply from two source-to-sink systems through two different channels.

5.3.2. Evolution of the Provenance System and its Implication for Tectonics

In Section 5.3.1, the samples from the same period were divided into different source-to-sink systems. On this basis, this study discusses the evolution of three source-to-sink systems, namely, the CMS system, the SMS system, and the ZU system. The samples from the same source-to-sink system were sorted according to the time series. Based on the changes in zircon age records, the recorded geological events were inferred to indicate the tectonic evolution (Figure 12). Since data on the Lower Wuerhe Formation were the only available data for the NMS system, the evolution of this provenance system is not discussed.

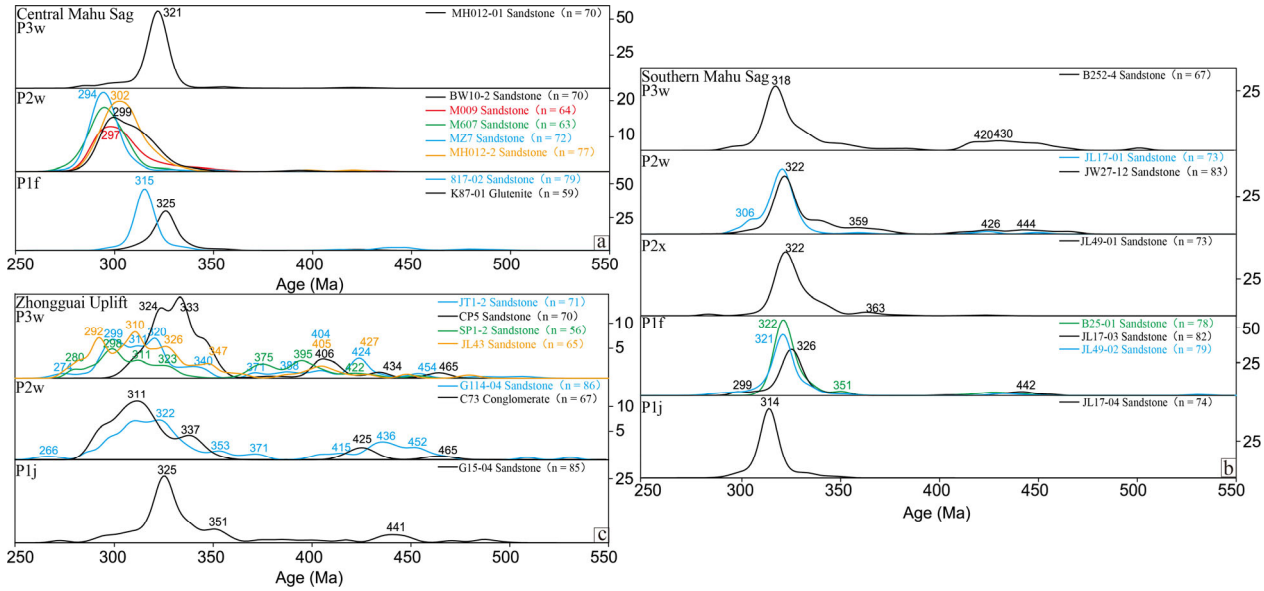

Figure 12. Distribution of the U-Pb ages of Permian detrital zircons over time. **(a)** The source-to-sink system CWJ→CMS in the central Mahu Sag (CMS). **(b)** The source-to-sink system CWJ + NWJ→SMS in the southern Mahu Sag (SMS). **(c)** The source-to-sink system CWJ + SWJ→ZU in the Zhongguai uplift (ZU). The strata become younger from bottom to top.

1. CWJ→CMS system in the CMS (Figure 12a)

Samples from the Jiamuhe Formation and the Xiazijie Formation were lacking. Throughout the Permian, the zircon age distribution of each sample was similar, with only one dominant peak in the Late Carboniferous, indicating a relatively simple source (mainly CWJ), a relatively limited provenance, and no large changes in the Permian.

2. CWJ + NWJ→SMS system in the SMS (Figure 12b)

The samples from the five Permian formations were relatively complete. The zircon age distribution patterns mostly possessed only a single Carboniferous peak and occasionally showed secondary peaks. No Silurian-Ordovician detrital zircons were present in the samples during the depositional period of the Jiamuhe Formation, whereas the content of older zircons in the samples gradually increased during and after the depositional period of the Fengcheng Formation. This finding indicates that the Junggar Basin did not receive any sediment supply from NWJ in the early stage of the Early Permian perhaps because of a drainage divide between NWJ and the Junggar Basin, and NWJ and the Junggar Basin were not connected until the late stage of the Early Permian. Compared with the lower Permian-Middle Permian samples, the samples formed during the depositional periods of the Lower Wuerhe and Upper Wuerhe Formations showed significantly higher proportions of the dated points in the intervals 270–300 Ma and 400–430 Ma and more complex distributions of detrital zircon ages. It is speculated that compressive thrusts developed in the West Junggar between the Middle Permian and the Early Triassic [9] resulted in the continuous overthrust nappe of the thrust-nappe system along the piedmont fault zone, further uplifting the provenances [7,20]. As a result, the proportion of the sediment supply from NWJ increased, and the Permian plutonic granite and diabase intrusions and the Devonian and Silurian series were uplifted to the surface and denudated (Figure 12).

3. CWJ + SWJ→ZU system in the ZU (Figure 12c)

There was a lack of samples from the Fengcheng Formation and the Xiazijie Formation. Compared with the samples from the Jiamuhe Formation, the samples from the Lower Wuerhe Formation and the Upper Wuerhe Formation showed significantly more complex distributions of detrital zircon ages, with broader ranges, more secondary peaks, and higher proportions of points dated in the 270–300 Ma and 370–465 Ma peaks, indicating increased sediment supply from SWJ. This finding reveals the accretionary orogeny on the southwestern margin of the CAOB during the Late Paleozoic [6,9] further increased the sediment supply from the Permian intermediate-felsic intrusive rocks and mafic dikes of CWJ and the Devonian-Ordovician rocks of SWJ into the strata of the study area.

Comparing the detrital zircon characteristics of the Middle-Upper Permian and the Lower-Middle Permian, the tectonic-sedimentary response of the ZU system was more pronounced than that of the SMS system (Figure 12). However, the CMS system has almost no obvious change. The CMS system is located on the short axis of the Mahu Sag, mainly receiving the provenance supply from the CWJ nearby. The ZU system and SMS system are adjacent to each other and are located on the long axis of the Mahu Sag. In addition to the main proximal provenance, they also receive the supply of distal sediments. Therefore, it is speculated that the latter's corresponding source areas in the SWJ and NWJ have a similar response to the accretionary orogeny of the West Junggar in the Late Paleozoic, and the response in the SWJ is more severe.

In particular, the Late Permian-Early Triassic period was an important transition period in the evolution of the basin. Two large regional unconformities were mainly developed between the Upper Permian-Lower Triassic and Upper Wuerhe Formation-Lower Wuerhe Formation in the northwestern margin of the Junggar Basin [3,6,9,18,146,147]. The SMS (Figure 12b) and the ZU (Figure 12c) showed more complex age distributions of Upper Permian detrital zircons in this period than in the Middle Permian, which may be related to the regional unconformity developed during the P_3w/P_2w transition period [73]. This unconformity developed due to the stratigraphic overlap during the transition from

rift to depression basin [148]. Moreover, during the deposition period of the Lower Wuerhe Formation, the age distribution of detrital zircon in the SMS and the ZU changed slightly. Except for the weathering and denudation of the old strata in the source area, it is speculated that the tectonic inversion occurred at the end of the Permian [20], which may be earlier than the Upper Wuerhe Formation in the Late Permian.

6. Conclusions

1. The results of sandstone detrital zircon U-Pb dating showed that the NMS in the Permian was characterized by a dominant peak at 310–330 Ma and a secondary peak at 400–440 Ma. The CMS showed only one single peak at 295–325 Ma. The SMS and the ZU exhibited multimodal distributions of zircon ages in the two intervals of 270–350 Ma and 370–450 Ma. In addition, lithic clasts are abundant in sandstones with low compositional and textural maturity, indicative of proximal source areas. Thus, the source of the Mahu-Zhongguai area was mainly the adjacent Carboniferous magmatic rocks and the Early Permian intrusions in CWJ. The Mahu-Zhongguai area developed four major source-to-sink systems in the Permian: the CWJ + NWJ→NMS system with CWJ and NWJ as the provenances and the NMS as the depositional area, the CWJ→CMS system with CWJ as the provenance and the CMS as the depositional area, the CWJ + NWJ→SMS system with CWJ and NWJ as the provenances and the SMS as the depositional area, and the CWJ + SWJ→ZU system with CWJ and SWJ as the provenances and the ZU as the depositional area.

2. Compared with the Early-Middle Permian, the detrital zircon ages showed a wider range and more peaks in the Lower Wuerhe and Upper Wuerhe Formations. This finding indicated the accretionary orogeny on the southwestern margin of the CAOB during the Late Paleozoic. The Permian intermediate-felsic intrusions and the Devonian and Silurian series in West Junggar uplifted (to the surface) and underwent denudation, thereby increasing the proportion of the sediment supply from SWJ and NWJ. The tectonic inversion may occur early in the Lower Wuerhe Formation and the response to tectonic activity is stronger in the SWJ than in the NWJ. Moreover, the provenance system of the Upper Wuerhe Formation was more complicated than before, which was speculated to be related to the regional unconformity of the transition and development of the properties of the Junggar Basin during the same period.

Supplementary Materials: The following supporting information can be downloaded at: www.mdpi.com/article/10.3390/min12091169/s1, Table S1: LA-ICP-MS detrital zircon U-Pb isotope analysis results of the Mahu-Zhongguai area on the northwestern margin of the Junggar Basin during the Permian. Table S2: The zircon-tourmaline-rutile (ZTR) index of the Lower Wuerhe Formation in the Mahu-Zhongguai area on the northwestern margin of the Junggar Basin. Table S3 LA-ICP-MS detrital zircon rare earth element (REE) analysis results of the Mahu-Zhongguai area on the northwestern margin of the Junggar Basin during the Permian.

Author Contributions: Conceptualization, X.C. and Z.Z.; methodology, X.C. and D.C.; validation, X.C.; formal analysis, X.C.; investigation, X.C. and C.Z.; resources, D.C.; writing—original draft preparation, X.C.; writing—review and editing, Z.Z. and L.W.; visualization, X.C.; supervision, Z.Z. and Y.L.; project administration, Z.Z. and C.Z.; funding acquisition, X.Y. All authors have read and agreed to the published version of the manuscript.

Funding: This work was supported by the National Science and Technology Major Project, grant number 2017ZX05001; the China National Petroleum Corporation Research Project, grant number 2019B0307, 2021DJ0401.

Data Availability Statement: Not applicable.

Acknowledgments: The authors thank Fan Chao of the State Key Laboratory of Continental Dynamics of Northwest University for the zircon U-Pb dating tests. We thank anonymous reviewers for sharing their valuable opinions.

Conflicts of Interest: The authors declare no conflict of interest.

Appendix A Method of Zircon U-Pb Dating

Crack-free zircon grains with smooth surfaces, good crystal shapes, and high transparency were selected for the preliminary transmitted light, reflected light, and cathodoluminescence (CL) photography. CL images were photographed by a scanning electron microscope (Gatan MonoCL3 + X). For each sample, 100 zircon grains were randomly selected for U-Pb dating.

Laser sampling was performed using a RESOlution S155-LR 193 nm laser ablation system coupled to an Agilent 7900 ICP–MS. The laser spot size was 40 μm in diameter, the shot frequency was 5 Hz, and the energy density was 6 J cm^{-2}. The ablated materials were conveyed into the ICP–MS by a stream of high-purity helium gas with a flux of 280 mL/min. The sampling method was single-point ablation and the data acquisition mode was peak jumping (20 ms per isotope for each cycle). The procedure for individual analysis included 10 s for the blank, 40 s for ablation and 20 s for flush. Raw count rates were measured for ^{29}Si, ^{204}Pb, ^{206}Pb, ^{207}Pb, ^{208}Pb, ^{232}Th and ^{238}U. The international standard zircon GJ-1 was used as the external standard for zircon age calculation, and the element content was corrected using the National Institute of Standards and Technology (NIST) SRM610 as the external standard and ^{29}Si as the internal standard isotope. Besides, Plešovice was used as the secondary standard to monitor the deviation of age. During the analyses, GJ-1 zircon samples were measured twice every eight analyses to correct for instrument drift, Plešovice zircons were measured once every eight analyses to assess the quality of the analyses, and SRM 610 were measured once every eight analyses.

The standard deviation of the isotope ratio and age of a single analysis point was 1σ, and the weighted average age was 2σ. The $^{207}Pb/^{206}Pb$ age was used for zircons older than 1000 Ma, while the $^{206}Pb/^{238}$ U age was used for zircons aged less than 1000 Ma [149]. The concordance is defined as 100% × (^{206}Pb–^{238}U age)/(^{207}Pb–^{206}Pb age) for the former analyses and 100% × (^{206}Pb–^{238}U age)/(^{207}Pb–^{235}U age) for the latter. For the detrital zircons, individual analyses with concordant percentages higher than 90% were chosen for calculation. The data were processed using ICPMSDataCal 11.8 software. Andersen's [150] software was used for common lead correction, and Isoplot 2.49 was used to calculate ages and generate Concordia plots. Analytical details for age and trace and rare earth element determinations of zircons are reported in Yuan et al. [151].

References

1. Xiao, X.C.; Tang, Y.Q.; Feng, Y.M.; Zhu, B.Q.; Li, J.Y.; Zhao, M. *Tectionic Evolution of Northern XinJiang and its Adjacent Regions*; Geological Publishing House: Beijing, China, 1992, pp. 1–169.
2. Sun, Z.C. Mesozoic-Cenozoic Foreland Basins and Their Hydrocarbon Prospect in Middle and Western Parts of China, as well as Division of Internal Texture Units in Gunggar Basin. *Marin. Orig. Petrl. Geol.* **1998**, *3*, 16–30
3. Chen, X.; Lu, H.F.; Shu, L.S.; Wang, H.M.; Zhang, G.Q. Study on Tectonic Evolution of Junggar Basin. *Geol. J. China Univ.* **2002**, *8*, 257–267. https://doi.org/10.3969/j.issn.1006-7493.2002.03.003.
4. Wu, Q.F. Structural evolution and prospects of Junggar Basin. *Xinjiang Geol.* **1986**, *4*, 1–19.
5. Chen, F.J.; Wang, X.W.; Wang, X.W. Prototype and tectonic evolution of the Junggar Basin, northwestern China. *Earth Sci. Front.* **2005**, *12*, 77–89. https://doi.org/10.3321/j.issn:1005-2321.2005.03.010.
6. He, D.F.; Zhang, L.; Wu, S.T.; Li, D.; Zhen, Y. Tectonic evolution stages and features of the Junggar Basin. *Oil Gas. Geol.* **2018**, *39*, 845–861. https://doi.org/10.11743/ogg20180501.
7. Tang, W.B.; Zhang, Y.Y.; Pe-Piper, G.; Piper, D.J.W.; Guo, Z.J.; Li, W. Permian to early Triassic tectono-sedimentary evolution of the Mahu sag, Junggar Basin, western China: Sedimentological implications of the transition from rifting to tectonic inversion. *Mar. Pet. Geol.* **2021**, *123*. https://doi.org/10.1016/j.marpetgeo.2020.104730.
8. Liang, Y.Y.; Zhang, Y.Y.; Chen, S.; Guo, Z.J.; Tang, W.B. Controls of a strike-slip fault system on the tectonic inversion of the Mahu depression at the northwestern margin of the Junggar Basin, NW China. *J. Asian Earth Sci.* **2020**, *198*, 104229. https://doi.org/10.1016/j.jseaes.2020.104229.
9. He, D.F.; Wu, S.T.; Zhao, L.; Zheng, M.L.; Li, D.; Lu, Y. Tectono-Depositional Setting and Its Evolution during Permian to Triassic around Mahu Sag, Junggar Basin. *Xinjiang Pet. Geol.* **2018**, *39*, 35–47. https://doi.org/10.7657/XJPG20180105.
10. Yu, Y.J.; Hu, S.Y.; He, D.F. Skeleton components of Permian-Lower Jurassic clastic rocks in NW margin of Junggar basin: Tracing to provenance and tectonic settings evolution. *Acta Geol. Sin.* **2020**, *94*, 1347–1366. https://doi.org/10.3969/j.issn.0001-5717.2020.05.002.

11. Dickinson, W.R.; Gehrels, G.E. U-Pb ages of detrital zircons from Permian and Jurassic eolian sandstones of the Colorado Plateau, USA: Paleogeographic implications. *Sediment. Geol.* **2003**, *163*, 29–66. https://doi.org/10.1016/S0037-0738(03)00158-1.
12. Romans, B.W.; Castelltort, S.; Covault, J.A.; Fildani, A.; Walsh, J.P. Environmental signal propagation in sedimentary systems across timescales. *Earth-Sci. Rev.* **2016**, *153*, 7–29. https://doi.org/10.1016/j.earscirev.2015.07.012.
13. Wu, W.; Li, Q.; Pei, J.X.; Ning, S.Y.; Tong, L.Q.; Liu, W.Q.; Feng, Z.D. Seismic sedimentology, facies analyses, and high-quality reservoir predictions in fan deltas: A case study of the Triassic Baikouquan Formation on the western slope of the Mahu Sag in China's Junggar Basin. *Mar. Pet. Geol.* **2020**, *120*, 104546. https://doi.org/10.1016/j.marpetgeo.2020.104546.
14. Feng, C.; Lei, D.W.; Qu, J.H.; Huo, J.Z. Controls of paleo-overpressure, faults and sedimentary facies on the distribution of the high pressure and high production oil pools in the lower Triassic Baikouquan Formation of the Mahu Sag, Junggar Basin, China. *J. Pet. Sci. Eng.* **2019**, *176*, 232–248. https://doi.org/10.1016/j.petrol.2019.01.012.
15. Li, J.; Tang, Y.; Wu, T.; Zhao, J.Z.; Wu, H.Y.; Wu, W.T.; Bai, Y.B. Overpressure origin and its effects on petroleum accumulation in the conglomerate oil province in Mahu Sag, Junggar Basin, NW China. *Pet. Explor. Dev.* **2020**, *47*, 726–739. https://doi.org/10.1016/S1876-3804(20)60088-X.
16. Zhang, C.M.; Yin, T.J.; Tang, Y.; Guo, X.G.; Zhao, K.; Pan, J.; Chen, M.L. Advances in sedimentological reservoir research in Mahu sag and northwest margin of Junggar Basin. *J. Palaeogeogr.* **2020**, *22*, 129–146. https://doi.org/10.7605/gdlxb.2020.01.008.
17. Zhang, C.M.; Song, X.M.; Wang, X.J.; Wang, X.L.; Zhao, K.; Shuang, Q.; Li, S.H. Origin and depositional characteristics of supported conglomerates. *Pet. Explor. Dev.* **2020**, *47*, 292–305. https://doi.org/10.1016/S1876-3804(20)60047-7.
18. Tang, Y.; Xu, Y.; Li, Y.Z.; Wang, L.B. Sedimentation Model and Exploration Significance of Large-Scaled Shallow Retrogradation Fan Delta in Mahu Sag. *Xinjiang Pet. Geol.* **2018**, *39*, 16–22. https://doi.org/10.7657/XJPG20180103.
19. Huang, Y.F.; Zhang, C.M.; Zhu, R.; Yi, X.F.; Qu, J.H.; Tang, Y. Palaeoclimatology, Provenance and Tectonic Setting during Late Permian to Middle Triassic in Mahu Sag, Junggar Basin, China. *Earth Sci.* **2017**, *42*, 1736–1749. https://doi.org/10.3799/dqkx.2017.559.
20. Tang, W.B.; Zhang, Y.Y.; Pe-Piper, G.; Piper, D.J.W.; Guo, Z.J.; Li, W. Permian rifting processes in the NW Junggar Basin, China: Implications for the post-accretionary successor basins. *Gondwana Res.* **2021**, *98*, 107–124. https://doi.org/10.1016/j.gr.2021.06.005.
21. Degraaff-Surpless, K.; Graham, S.A.; Wooden, J.L.; Mcwilliams, M.O. Detrital zircon provenance analysis of the Great Valley Group, California: Evolution of an arc-forearc system. *Geol. Soc. Am. Bull.* **2002**, *114*, 1564–1580. https://doi.org/10.1130/0016-7606(2002)114<1564:Dzpaot>2.0.Co;2.
22. Fonneland, H.C.; Lien, T.; Martinsen, O.J.; Pedersen, R.B.; Kosler, J. Detrital zircon ages: A key to understanding the deposition of deep marine sandstones in the Norwegian Sea. *Sediment. Geol.* **2004**, *164*, 147–159. https://doi.org/10.1016/j.sedgeo.2003.09.005.
23. He, D.F.; Li, D.; Fan, C.; Yang, X.F. Geochronology, geochemistry and tectonostratigraphy of Carboniferous strata of the deepest Well Moshen-1 in the Junggar Basin, northwest China: Insights into the continental growth of Central Asia. *Gondwana Res.* **2013**, *24*, 560–577. https://doi.org/10.1016/j.gr.2012.10.015.
24. Xu, X.Y.; Li, R.S.; Chen, J.L.; Ma, Z.P.; Li, Z.P.; Wang, H.L.; Bai, J.K.; Tang, Z. New constrains on the Paleozoic tectonic evolution of the northern Xinjiang area. *Acta Petrol. Sin.* **2014**, *30*, 1521–1534.
25. Feng, T.R. Permian Tectono-Stratigraphic Sequence and Basin Evolution in Junggar Basin. MA Thesis, China University of Geosciences, Beijing, China, 2017-05.
26. Sun, G.Q.; Shi, J.A.; Zhang, S.C.; Chen, J.; Jia, Y.Y. Geochemical characteristics and tectonic setting of the Carboniferous-Permian volcanic rocks in Zhongguai area northwestern Junggar Basin. *Chin. J. Geol.* **2012**, *47*, 993–1004. https://doi.org/10.3969/j.issn.0563-5020.2012.04.005.
27. Mao, X.; Li, J.H.; Zhang, H.T.; Wang, L. Study on the distribution and developmental environment of the Late Paleozoic volcanoes in Junggar Basin and its adjacent areas. *Acta Petrol. Sin.* **2012**, *28*, 2381–2391.
28. Xu, Z.; Han, B.F.; Ren, R.; Zhou, Y.Z.; Su, L. Palaeozoic multiphase magmatism at Barleik Mountain, southern West Junggar, Northwest China: Implications for tectonic evolution of the West Junggar. *Int. Geol. Rev.* **2012**, *55*, 633–656. https://doi.org/10.1080/00206814.2012.741315.
29. Liu, B.; Han, B.F.; Chen, J.F.; Ren, R.; Zheng, B.; Wang, Z.Z.; Feng, L.X. Closure Time of the Junggar-Balkhash Ocean: Constraints from Late Paleozoic Volcano-Sedimentary Sequences in the Barleik Mountains, West Junggar, NW China. *Tectonics* **2017**, *36*, 2823–2845. https://doi.org/10.1002/2017tc004606.
30. Zheng, R.G.; Zhao, L.; Yang, Y.Q. Geochronology, geochemistry and tectonic implications of a new ophiolitic melange in the northern West Junggar, NW China. *Gondwana Res.* **2019**, *74*, 237–250. https://doi.org/10.1016/j.gr.2019.01.008.
31. Yang, Y.Q.; Zhao, L.; Zheng, R.G.; Xu, Q.Q. Evolution of the early Paleozoic Hongguleleng-Balkybey Ocean: Evidence from the Hebukesaier ophiolitic melange in the northern West Junggar, NW China. *Lithos* **2019**, *324*, 519–536. https://doi.org/10.1016/j.lithos.2018.11.029.
32. Zhang, Y.Y.; Guo, Z.J. New Constraints on Formation Ages of Ophiolites In Northern Junggar and Comparative Study On their Connection. *Acta Petrol. Sin.* **2010**, *26*, 422–430.
33. Du, H.Y.; Chen, J.F. The Determination of Hoboksar Ancient Oceanic Basin in West Junngar: Evidence from Zircon U-Pb Age and Geochemistry of the Hoboksar Ophiolitic Mélange. *Acta Geol. Sin.* **2017**, *91*, 2638–2650. https://doi.org/10.3969/j.issn.0001-5717.2017.12.004.

34. Chen, J.F.; Han, B.F.; Zhang, L. Geochemistry,Sr-Nd isotopes and tectonic implications of two generations of Late Paleozoic plutons in northern West Junggar,Northwest China. *Acta Petrol. Sin.* **2010**, *26*, 2317–2335.
35. Zheng, B.; Han, B.F.; Liu, B.; Wang, Z.Z. Ediacaran to Paleozoic magmatism in West Junggar Orogenic Belt, NW China, and implications for evolution of Central Asian Orogenic Belt. *Lithos* **2019**, *338*, 111–127. https://doi.org/10.1016/j.lithos.2019.04.017.
36. Shen, P.; Shen, Y.C.; Liu, T.B.; Li, G.M.; Zeng, Q.D. Geology and geochemistry of the Early Carboniferous Eastern Sawur caldera complex and associated gold epithermal mineralization, Sawur Mountains, Xinjiang, China. *J. Asian Earth Sci.* **2008**, *32*, 259–279. https://doi.org/10.1016/j.jseaes.2007.10.004.
37. Chen, J.F.; Han, B.F.; Ji, J.Q.; Zhang, L.; Xu, Z.; He, G.Q.; Wang, T. Zircon U-Pb ages and tectonic implications of Paleozoic plutons in northern West Junggar, North Xinjiang, China. *Lithos* **2010**, *115*, 137–152. https://doi.org/10.1016/j.lithos.2009.11.014.
38. Zhu, Y.F.; Xu, X. The Discovery of Early Ordovician Ophiolite Mélange in Taerbahatai Mts., Xinjiang, NW China. *Acta Petrol. Sin.* **2006**, 2833-2842. https://doi.org/10.3321/j.issn:1000-0569.2006.12.002.
39. Choulet, F.; Faure, M.; Cluzel, D.; Chen, Y.; Lin, W.; Wang, B.; Jahn, B.M. Architecture and evolution of accretionary orogens in the Altaids collage: The early Paleozoic West Junggar (NW China). *Am. J. Sci.* **2013**, *312*, 1098–1145. https://doi.org/10.2475/10.2012.02.
40. Wang, Z.Q. Volcanic Rock Strata in the Xiemisitai Area of West Junggar. Xinjiang. MA Thesis, China University of Geosciences, Beijing, China, 2015-06.
41. Yang, G.X.; Li, Y.J.; Santosh, M.; Yang, B.K.; Zhang, B.; Tong, L.L. Geochronology and geochemistry of basalts from the Karamay ophiolitic melange in West Junggar (NW China): Implications for Devonian-Carboniferous intra-oceanic accretionary tectonics of the southern Altaids. *Geol. Soc. Am. Bull.* **2013**, *125*, 401–419. https://doi.org/10.1130/B30650.1.
42. Yang, G.X.; Li, Y.J.; Gu, P.Y.; Yang, B.K.; Tong, L.L.; Zhang, H.W. Geochronological and geochemical study of the Darbut Ophiolitic Complex in the West Junggar (NW China): Implications for petrogenesis and tectonic evolution. *Gondwana Res.* **2012**, *21*, 1037–1049. https://doi.org/10.1016/j.gr.2011.07.029.
43. Chen, S.; Guo, Z.J.; Pe-Piper, G.; Zhu, B.B. Late Paleozoic peperites in West Junggar, China, and how they constrain regional tectonic and palaeoenvironmental setting. *Gondwana Res.* **2013**, *23*, 666–681. https://doi.org/10.1016/j.gr.2012.04.012.
44. Liu, Y.; Wang, X.; Wu, K.Y.; Chen, S.N.; Shi, Z.; Yao, W.J. Late Carboniferous seismic and volcanic record in the northwestern margin of the Junggar Basin: Implication for the tectonic setting of the West Junggar. *Gondwana Res.* **2019**, *71*, 49–75. https://doi.org/10.1016/j.gr.2019.01.013.
45. Gao, R.; Xiao, L.; Pirajno, F.; Wang, G.C.; He, X.X.; Yang, G.; Yan, S.W. Carboniferous-Permian extensive magmatism in the West Junggar, Xinjiang, northwestern China: Its geochemistry, geochronology, and petrogenesis. *Lithos* **2014**, *204*, 125–143. https://doi.org/10.1016/j.lithos.2014.05.028.
46. Duan, F.H.; Li, Y.J.; Zhi, Q. Late Paleozoic multi-stage subduction accretion of the southwestern Central Asian Orogenic Belt: Insights from the Late Carboniferous-Early Permian granites in the southern West Junggar, NW China. *Int. Geol. Rev.* **2022**, *64*, 2051–2073. https://doi.org/10.1080/00206814.2021.1969526.
47. Xu, Z.; Han, B.F.; Ren, R.; Zhou, Y.Z.; Zhang, L.; Chen, J.F.; Su, L.; Li, X.H.; Liu, D.Y. Ultramafic-mafic melange, island arc and post-collisional intrusions in the Mayile Mountain, West Junggar, China: Implications for Paleozoic intra-oceanic subduction-accretion process. *Lithos* **2012**, *132*, 141–161. https://doi.org/10.1016/j.lithos.2011.11.016.
48. Liu, B.; Han, B.F. Identification of lateral inhomogeneity of arc basement by reconstructing the Late Devonian arc belt in the southwestern Central Asian Orogenic Belt. *J. Geodyn.* **2019**, *132*, 101668. https://doi.org/10.1016/j.jog.2019.101668.
49. Yang, G.X.; Li, Y.J.; Santosh, M.; Xiao, W.J.; Yang, B.K.; Tong, L.L.; Zhang, S.L. Alkaline basalts in the Karamay ophiolitic melange, NW China: A geological, geochemical and geochronological study and implications for geodynamic setting. *J. Asian Earth Sci.* **2015**, *113*, 110–125. https://doi.org/10.1016/j.jseaes.2014.08.017.
50. Liu, B.; Han, B.F.; Ren, R.; Zheng, B.; Chen, J.F.; Xiao, W. Late Carboniferous to Early Permian adakitic rocks and fractionated I-type granites in the southern West Junggar terrane, NW China: Implications for the final closure of the Junggar–Balkhash Ocean. *Geol. J.* **2020**, *55*, 1728–1749. https://doi.org/10.1002/gj.3508.
51. Ren, R.; Han, B.F.; Guan, S.W.; Liu, B.; Wang, Z.Z. Linking the southern West Junggar terrane to the Yili Block: Insights from the oldest accretionary complexes in West Junggar, NW China. *J. Asian Earth Sci.* **2018**, *159*, 279–293. https://doi.org/10.1016/j.jseaes.2017.03.011.
52. Ren, R.; Han, B.F.; Xu, Z.; Zhou, Y.Z.; Liu, B.; Zhang, L.; Chen, J.F.; Su, L.; Li, J.; Li, X.H.; et al. When did the subduction first initiate in the southern Paleo-Asian Ocean: New constraints from a Cambrian intra-oceanic arc system in West Junggar, NW China. *Earth Planet. Sci. Lett.* **2014**, *388*, 222–236. https://doi.org/10.1016/j.epsl.2013.11.055.
53. Choulet, F.; Cluzel, D.; Faure, M.; Lin, W.; Wang, B.; Chen, Y.; Wu, F.Y.; Ji, W.B. New constraints on the pre-Permian continental crust growth of Central Asia (West Junggar, China) by U-Pb and Hf isotopic data from detrital zircon. *Terra Nova* **2012**, *24*, 189–198. https://doi.org/10.1111/j.1365-3121.2011.01052.x.
54. Yang, G.X. Geological Characteristics and Tectonic Evolution of Paleozoic Ophiolitic Mélange in the West Junggar, Ph.D. Thesis, Chang'an University, Xi'an, China, 9 May 2012
55. Tang, Y.; Hou, Z.S.; Wang, X.T.; Wang, T.; Wu, Q.; Shen, B.H.; Wang, W.Q.; Zhang, H.; Cao, J.; Zhang, S.C.; et al. Progress of the Carboniferous and Permian stratigraphic framework and correlation of the Junggar Basin, Xinjiang, Northwest China. *Geol. Rev.* **2022**, *68*, 385–407. https://doi.org/10.16509/j.georeview.2022.01.011.

56. He, H.; Li, S.M.; Liu, C.; Kong, C.X.; Jiang, Q.P.; Chang, T.Q. Characteristics and quantitative evaluation of volcanic effective reservoirs: A case study from Junggar Basin, China. *J. Pet. Sci. Eng.* **2020**, *195*, 107723. https://doi.org/10.1016/j.petrol.2020.107723.
57. Xia, L.W.; Cao, J.; Stueken, E.E.; Zhi, D.M.; Wang, T.T.; Li, W.W. Unsynchronized evolution of salinity and pH of a Permian alkaline lake influenced by hydrothermal fluids: A multi-proxy geochemical study. *Chem. Geol.* **2020**, *541*, 119581. https://doi.org/10.1016/j.chemgeo.2020.119581.
58. Tang, W.B.; Zhang, Y.Y.; Pe-Piper, G.; Piper, D.J.W.; Guo, Z.J.; Li, W. Soft-sediment deformation structures in alkaline lake deposits of Lower Permian Fengcheng Formation, Junggar Basin, NW China: Implications for syn-sedimentary tectonic activity. *Sediment. Geol.* **2020**, *406*, 105719. https://doi.org/10.1016/j.sedgeo.2020.105719.
59. Cao, J.; Xia, L.W.; Wang, T.T.; Zhi, D.M.; Tang, Y.; Li, W.W. An alkaline lake in the Late Paleozoic Ice Age (LPIA): A review and new insights into paleoenvironment and petroleum geology. *Earth-Sci. Rev.* **2020**, *202*, 103091. https://doi.org/10.1016/j.earscirev.2020.103091.
60. Zhang, Z.J.; Yuan, X.J.; Wang, M.S.; Zhou, C.M.; Tang, Y.; Chen, X.Y.; Lin, M.J.; Cheng, D.W. Alkaline-lacustrine deposition and paleoenvironmental evolution in Permian Fengcheng Formation at the Mahu sag, Junggar Basin, NW China. *Pet. Explor. Dev.* **2018**, *45*, 1036–1049. https://doi.org/10.1016/S1876-3804(18)30107-1.
61. Cao, J.; Lei, D.W.; Li, Y.W.; Tang, Y.; Chang, Q.S.; Abulimit, Wang, T.T. Ancient high-quality alkaline lacustrine source rocks discovered in the Lower Permian Fengcheng Formation, Junggar Basin. *Acta Pet. Sin.* **2015**, *36*, 781–790. https://doi.org/10.7623/syxb201507002.
62. Yang, F.; Bian, B.L.; Liu, H.Y.; Yao, Z.Q.; You, X.C.; Liu, H.L.; Wei, Y.Z. Sedimentary characteristics of fan delta in restricted lacustrine basin of Permian Xiazijie Formation in Mahu Sag. *Lithol. Reserv.* **2022**, *34*, 63–72. https://doi.org/10.12108/yxyqc.20220505.
63. Ma, Y.P.; Wang, G.D.; Zhang, X.W.; Pan, S.X.; Huang, L.J.; Chen, Y.B.; Guo, J.J. Development model of secondary pores in coarse-grained deposits: A case study of Permian Xiazijie Formation in northwestern margin of Junggar Basin. *Lithol. Reserv.* **2019**, *31*, 34–43. https://doi.org/10.12108/yxyqc.20190504.
64. Zhu, S.Q.; Xiao, C.L.; Rao, Z.; Kuang, H.W.; Xing, F.C.; Gao, Z.Z. Fluvial-dominated fan delta sedimentation of the Lower Urho Formation of Upper Permian in the 8th Area of Karamay Oilfield, Xinjiang Autonomous Region. *J. Palaeogeogr.* **2005**, *7*, 471–482. https://doi.org/10.3969/j.issn.1671-1505.2005.04.005.
65. Yang, F.; Wei, Y.Z.; Abu, L.M.T.; Chen, G.Q.; Bian, B.L. Optimization of Favorable Reservoir-Caprock Assemblages of Middle-Upper Permian in Mahu Sag, Junggar Basin. *Xinjiang Pet. Geol.* **2016**, *37*, 131–137. https://doi.org/10.7657/XJPG20160202.
66. Zou, Z.W.; Guo, H.J.; Niu, Z.J.; Xu, Y.; Shan, X.; Li, Y.Z.; Shen, J.L. Sedimentary characteristics and controlling factors of river-dominated fan delta: A case study from the Upper Urho Formation in Mahu sag of Junggar Basin. *J. Palaeogeogr.* **2021**, *23*, 756–770. https://doi.org/10.7605/gdlxb.2021.04.049.
67. Ma, Y.P.; Zhang, X.W.; Zhu, K.; Wang, G.D.; Pan, S.X.; Huang, L.J.; Zhang, H.; Guan, X. Sedimentary characteristics and controlling factors of fan-delta of the Upper Urho Formation of Permian in Mahu Sag. *Lithol. Reserv.* **2021**, *33*, 57–70. https://doi.org/10.12108/yxyqc.20210106.
68. Yu, H.T.; Liu, X.Y.; Wu, B.W.; Liu, X.M. Large Fan Delta Control Factors of Upper Wuerhe Formation of Shawan Sag in Northwest Margin of Junggar Basin. *Xinjiang Geol.* **2020**, *38*, 71–76. https://doi.org/10.3969/j.issn.1000-8845.2020.01.012.
69. Cao, Z.L.; Li, P.; Wang, R.J. Sequence architecture, slope-break development and hydrocarbon implications of the Mahu Sag during the P-T transition, Junggar Basin. *Nat. Gas. Geosci.* **2022**, 33, 1–16. https://doi.org/10.11764/j.issn.1672-1926.2021.12.011.
70. Meng, X.C.; Qi, H.Y.; Chen, Y.; Xie, Z.R.; Dou, Y.; Xu, Y.; Guo, H.J. Genesis of low GR weathering paleosols and high GR glutenite and oil & gas exploration: A case study of the Upper Permian Wuerhe formation in Manan area. *J. China Univ. Min. Technol.* **2021**, *50*, 1153–1168.
71. Li, P.; Li, Y.Q.; Jing, J.B.; Cao, Z.L.; Yuan, X.J. Unconformities formed during the P-T transition in the northwestern Junggar Basin: Nature, evolution and implications. *J. Palaeogeogr.* **2020**, *22*, 697–714. https://doi.org/10.7605/gdlxb.2020.07.068.
72. Li, D. Carboniferous Tectonic Framework and Sedimentary Filling Evolution in the Junggar Basin and Adjacent Area, NW China. Ph.D. Thesis, China University of Geosciences, Beijing, China, June 2016
73. Lu, Y. Permian Chronostratigraphic Framework and Sedimentary Filling Evolution in Mahu-shawan and Adjacent Area, Junggar Basin. MA Thesis, China University of Geosciences, Beijing, China, May 2018
74. Sharman, G.R.; Sharman, J.P.; Sylvester, Z. detritalPy: A Python-based toolset for visualizing and analysing detrital geo-thermochronologic data. *Depos. Rec.* **2018**, *4*, 202–215. https://doi.org/10.1002/dep2.45.
75. Belousova, E.A.; Griffin, W.L.; O'reilly, S.Y.; Fisher, N.I. Apatite as an indicator mineral for mineral exploration: Trace-element compositions and their relationship to host rock type. *J. Geochem. Explor.* **2002**, *76*, 45–69. https://doi.org/10.1016/S0375-6742(02)00204-2.
76. Hoskin, P.W.O.; Ireland, T.R. Rare earth element chemistry of zircon and its use as a provenance indicator. *Geology* **2000**, *28*, 627–630. https://doi.org/10.1130/0091-7613(2000)028<0627:Reecoz>2.3.Co;2.
77. Hoskin, P.W.O.; Kinny, P.D.; Wyborn, D.; Chappell, B.W. Identifying accessory mineral saturation during differentiation in granitoid magmas: An integrated approach. *J. Pet.* **2000**, *41*, 1365–1396. https://doi.org/10.1093/petrology/41.9.1365.

78. Rubatto, D. Zircon trace element geochemistry: Partitioning with garnet and the link between U-Pb ages and metamorphism. *Chem. Geol.* **2002**, *184*, 123–138. https://doi.org/10.1016/S0009-2541(01)00355-2.
79. Sun, S.S.; Mcdonough, W.F. Chemical and isotopic systematics of oceanic basalts: Implications for mantle composition and processes. *Geol. Soc. London Sp. Publ.* **1989**, *42*, 313–345. https://doi.org/10.1144/GSL.SP.1989.042.01.19.
80. Li, H.Q.; Chen, F.W.; Cai, H. Study on Rb-Sr Isotopic Ages of Gold Deposits in West Junggar Area, Xinjiang. *Acta Geol. Sin.* **2000**, *74*, 181–192. https://doi.org/10.3321/j.issn:0001-5717.2000.02.009.
81. Li, X.Z.; Han, B.F.; Ji, J.Q.; Li, Z.H.; Liu, Z.Q.; Yang, B. Geology, geochemistry and K-Ar ages of the Karamay basic-intermediate dyke swarm from Xinjiang, China. *Geochimica* **2004**, *33*, 574–584. https://doi.org/10.3321/j.issn:0379-1726.2004.06.005.
82. Jian, P.; Li, D.Y.; Shi, Y.R.; Zhang, F.Q. SHRIMP dating of SSZ ophiolites from northern Xinjiang Province, China: Implications for generation of oceanic crust in the Central Asian Orogenic Belt. In *Structural and Tectonic Correlation Across the Central Asian Orogenic Collage: Northeastern Segment*; Sklyarov, E.V., Ed.; IEC SB RAS: Irkutsk, Russia, 2005; pp. 246–251.
83. Han, B.F.; Ji, J.Q.; Song, B.; Chen, L.H.; Zhang, L. Late Paleozoic vertical growth of continental crust around the Junggar Basin, Xinjiang, China (Part I): Timing of post-collisional plutonism. *Acta Petrol. Sin.* **2006**, *22*, 1077–1086. https://doi.org/10.3969/j.issn.1000-0569.2006.05.003.
84. Zhou, J.; Ji, J.Q.; Han, B.F.; Ma, F.; Gong, J.F.; Xu, Q.Q.; Guo, Z.J. 40Ar/39Ar Geochronology of mafic dykes in north Xinjiang. *Acta Petrol. Sin.* **2008**, *24*, 997–1010.
85. Geng, H.Y.; Sun, M.; Yuan, C.; Xiao, W.J.; Xian, W.S.; Zhao, G.C.; Zhang, L.F.; Wong, K.; Wu, F.Y. Geochemical, Sr–Nd and zircon U–Pb–Hf isotopic studies of Late Carboniferous magmatism in the West Junggar, Xinjiang: Implications for ridge subduction? *Chem. Geol.* **2009**, *266*, 364–389. https://doi.org/10.1016/j.chemgeo.2009.07.001.
86. Chen, J.F. Paleozoic Magmatism and Tectonic Evolution in Northern West Junggar, Xinjiang, China. Ph.D. Thesis, Peking University, Beijing, China, June 2011
87. Feng, Q.W.; Li, J.Y.; Liu, J.F.; Zhang, J.; Qu, J.F. Ages of the Hongshan granite and intruding dioritic dyke swarms, in western Junggar, Xinjiang, NW China: Evidence form LA-ICP-MS zircon chronology. *Acta Petrol. Sin.* **2012**, *28*, 2935–2949.
88. Feng, Q.W.; Li, J.Y.; Liu, J.F.; Song, B.; Wang, Y.B.; Chen, W.; Zhang, Y. Ages and geological siggnificance of the dark dykes emplaced in the Karamay pluton and adjacent area, in western Junggar, Xinjiang, NW China: Evidence form LAICP-MS zircon chronology and Ar-Ar amphibole chronology. *Acta Petrol. Sin.* **2012**, *28*, 2158–2170.
89. Shang, Z.C.; Wang, H.T.; Zhang, W.; Liu, K.X.; He, Y.B.; Wei, D.W. Geochronology and Tectonic Implications of the Granites in West Junggar, Xinjiang. *Gansu Geol.* **2012**, *21*, 1–5
90. Tang, G.J.; Wang, Q.; Wyman, D.A.; Li, Z.X.; Xu, Y.G.; Zhao, Z.H. Recycling oceanic crust for continental crustal growth: Sr–Nd–Hf isotope evidence from granitoids in the western Junggar region, NW China. *Lithos* **2012**, *128*, 73–83. https://doi.org/10.1016/j.lithos.2011.11.003.
91. Yang, G.X.; Li, Y.J.; Santosh, M.; Yang, B.K.; Yan, J.; Zhang, B.; Tong, L.L. Geochronology and geochemistry of basaltic rocks from the Sartuohai ophiolitic melange, NW China: Implications for a Devonian mantle plume within the Junggar Ocean. *J. Asian Earth Sci.* **2012**, *59*, 141–155. https://doi.org/10.1016/j.jseaes.2012.07.020.
92. Tian, Y.Z. Genesis of high-Al chromitite of the Sartohay ophiolite, Xinjiang. Ph.D. Thesis, Chinese Academy of Geological Sciences, Beijing, China, 13 April 2015
93. Xiang, K.P. Carboniferous sedimentary basin analysis and tectonic significance in the Baogutu-Halaalate Mountain, Western Junggar, Xinjiang. Ph.D. Thesis, Chang'an University, Xi'an, China, 2 June 2015
94. Zhang, R.F.; Yuan, F.; Zhou, T.F.; Deng, Y.F.; Zhang, D.Y.; Xu, C.; Zhao, B.B. Geological characteristics, geochronology and geochemical characteristics of volcanic hydrothermal type copper deposits (points) in Taerbahatai-xiemisitai region, West Junggar. *Acta Petrol. Sin.* **2015**, *31*, 2259–2276.
95. Jin, S. Study on Geochronology and Geochemistry of Paleozoic Magmatism in West Junggar area, Xinjiang. Ph.D. Thesis, China University of Geosciences, Wuhan, China, 2016-05.
96. Chen, W.F. Comparative Study on Late Paleozoic Tectonic-Magmatism Evolution in Eastern and Western Junggar, Xinjiang, Western China. Ph.D. Thesis, Lanzhou University, Lanzhou, China, May, 2017
97. Tang, G.J.; Chung, S.L.; Hawkesworth, C.J.; Cawood, P.A.; Wang, Q.; Wyman, D.A.; Xu, Y.G.; Zhao, Z.H. Short episodes of crust generation during protracted accretionary processes: Evidence from Central Asian Orogenic Belt, NW China. *Earth Planet. Sci. Lett.* **2017**, *464*, 142–154. https://doi.org/10.1016/j.epsl.2017.02.022.
98. Yin, J.Y.; Chen, W.; Xiao, W.J.; Yuan, C.; Windley, B.F.; Yu, S.; Cai, K. Late Silurian-early Devonian adakitic granodiorite, A-type and I-type granites in NW Junggar, NW China: Partial melting of mafic lower crust and implications for slab roll-back. *Gondwana Res.* **2017**, *43*, 55–73. https://doi.org/10.1016/j.gr.2015.06.016.
99. Yin, J.Y.; Chen, W.; Xiao, W.J.; Yuan, C.; Sun, M.; Cai, K.D. Petrogenesis and tectonic implications of early Devonian mafic dike–granite association in the northern West Junggar, NW China. *Int. Geol. Rev.* **2017**, *60*, 87–100. https://doi.org/10.1080/00206814.2017.1323238.
100. Duan, F.H. Carboniferous-Permian Magmatism and Tectonic Evolution in the Hatu-Baogutu Region of Southern West Junggar. Ph.D. Thesis, Chang'an University, Xi'an, China, 29 May 2018

101. Wang, Z.Q.; Jiang, X.M.; Guo, J.; Xu, F.; Deng, X.; Zhang, Q.; Li, J.; Niu, Q.Y.; Luo, Z.H. Discovery of the Early Paleozoic Volcanic Rocks in the Xiemisitai Area of the West Junggar, Xinjiang. *Geotecton. Metallog.* **2014**, *38*, 670–685. https://doi.org/10.3969/j.issn.1001-1552.2014.03.020.
102. Yi, S.X.; Li, Y.J.; Jiao, G.L.; Sun, Y.; Yang, G.X.; Wang, J.N.; Yang, F.Z. Geochemistry Characteristics of the Early Carboniferous Volcanic Rocks in the Boshchekul-Chingiz Volcanic Arc, West Junggar and Its Tectonic Implication. *Bull. Mineral., Petrol. Geochem.* **2014**, *33*, 431–438. https://doi.org/10.3969/j.issn.1007-2802.2014.04.003.
103. Yi, S.X.; Li, Y.J.; Jiao, G.L.; Yang, G.X.; Wang, J.N.; Yang, F.Z. The Establishment and Tectonic Settings Implication of Volcanic Rocks Which Belongs to the Early Carboniferous in the Boshchekul-Chingiz Volcanic Arc, West Junggar. *Xinjiang Geol.* **2014**, *32*, 14–18. https://doi.org/10.3969/j.issn.1000-8845.2014.01.003.
104. Yin, J.Y.; Chen, W.; Yuan, C.; Xiao, W.J.; Long, X.P.; Cai, K.D. Petrogenesis and Tectonic Implication of Early Carboniferous Basaltic Andesite in the Eastern Part of Xiemisitai Mountain, Northern West Junggar. *Geotecton. Metallog.* **2015**, *39*, 876–888. https://doi.org/10.16539/j.ddgzyckx.2015.05.011.
105. Tan, L.G.; Zhou, T.F.; Yuan, F.; Fan, Y.; Yue, S.C. Geodynamic Background of Permian Volcanic Rocks in the Sawuer Region, Xinjiang. *J. Hefei Univ. Technol. Nat. Sci.* **2006**, 29, 868–874.
106. Zhou, T.F.; Yuan, F.; Yang, W.P.; He, L.X.; Tan, L.G.; Fan, Y.; Yue, S.C. Permian Volcanism in the Sawu'er Area, Western Junggar. *Geol. China* **2006**, *33*, 553–558. https://doi.org/10.3969/j.issn.1000-3657.2006.03.011.
107. Weng, K.; Xu, X.Y.; Ma, Z.P.; Sun, J.M.; Zhang, T. U-Pb Zircon Dating and Geochimical Research of Devonian Volcanic Rocks in Urkashgar of Western Junggar. *Acta Geol. Sin.* **2013**, *87*, 515–524. https://doi.org/10.3969/j.issn.0001-5717.2013.04.006.
108. Xiang, K.P.; Li, Y.J.; Yang, Y.; Wang, R.; Sun, Y.; Yang, G.X.; Wang, J.N. Geochemistry of Volcanic Rocks from the Malasu Formation of Early Devonian in the West of Ur Kashgar Mountain, Western Junggar, and its Tectonic Implications. *J. Mineral. Petrol.* **2014**, *34*, 71–78.
109. Zhang, P.; Wang, G.C.; Shen, T.Y.; Polat, A.; Zhu, C.Y. Paleozoic convergence processes in the southwestern Central Asian Orogenic Belt: Insights from U-Pb dating of detrital zircons from West Junggar, northwestern China. *Geosci. Front.* **2021**, *12*, 531–548. https://doi.org/10.1016/j.gsf.2020.07.015.
110. Han, Y.G.; Zhao, G.C. Final amalgamation of the Tianshan and Junggar orogenic collage in the southwestern Central Asian Orogenic Belt: Constraints on the closure of the Paleo-Asian Ocean. *Earth-Sci. Rev.* **2018**, *186*, 129–152. https://doi.org/10.1016/j.earscirev.2017.09.012.
111. Zhang, C.; Santosh, M.; Liu, L.F.; Luo, Q.; Zhang, X.; Liu, D.D. Early Silurian to Early Carboniferous ridge subduction in NW Junggar: Evidence from geochronological, geochemical, and Sr-Nd-Hf isotopic data on alkali granites and adakites. *Lithos* **2018**, *300*, 314–329. https://doi.org/10.1016/j.lithos.2017.12.010.
112. Deng, Y.F.; Yuan, F.; Zhou, T.F.; Hollings, P.; Zhang, D.Y. Geochemistry and tectonic implications of the Early Carboniferous Keketuobie intrusion in the West Junggar foldbelt, NW China. *J. Asian Earth Sci.* **2018**, *159*, 142–154. https://doi.org/10.1016/j.jseaes.2017.09.014.
113. Chen, B.; Jahn, B.M. Genesis of post-collisional granitoids and basement nature of the Junggar Terrane, NW China: Nd-Sr isotope and trace element evidence. *J. Asian Earth Sci.* **2004**, *23*, 691–703. https://doi.org/10.1016/S1367-9120(03)00118-4.
114. Zhao, L.; He, G.Q.; Zhu, Y.B. Discovery and its Tectonic Significance of the Ophiolite in the South of Xiemisitai Mountain, West Junggar, Xinjiang. *Geol. Bull. China* **2013**, *32*, 195–205. https://doi.org/10.3969/j.issn.1671-2552.2013.01.019.
115. Zong, R.W.; Wang, Z.Z.; Gong, Y.M.; Wang, G.C.; Xiao, L.; Wang, Z.H.; Fan, R.Y. Ordovician radiolarians from the Yinisala ophiolitic mélange and their significance in western Junggar, Xinjiang, NW China. *Sci. China Earth Sci.* **2015**, *58*, 776–783. https://doi.org/10.1007/s11430-014-4974-5.
116. Xu, X.; He, G.Q.; Li, H.Q.; Ding, T.F.; Liu, X.Y.; Mei, S.W. Basic Characteristics of the Karamay Ophiolitic Mélange, Xinjiang, and Its Zircon SHRIMP Dating. *Geol. China* **2006**, *33*, 470–475. https://doi.org/10.3969/j.issn.1000-3657.2006.03.003.
117. Gu, P.Y.; Li, Y.J.; Zhang, B.; Tong, L.L.; Wang, J.N. LA-ICP-MS Zircon U-Pb Dating of Gabbro in the Darbut Ophiolite, Western Junggar, China. *Acta Petrol. Sin.* **2009**, *25*, 1364–1372.
118. Yang, G.X.; Li, Y.J.; Yang, B.K.; Liu, Z.W.; Tong, L.L.; Zhang, H.W. Zircon U-Pb Geochronology and Geochemistry of the Mayile Ophiolitic Mélange in West Junggar and Implications for Source Nature. *Acta Petrol. Sin.* **2013**, *29*, 303–316.
119. Li, D.; He, D.F.; Santosh, M.; Ma, D.L.; Tang, J.Y. Tectonic framework of the northern Junggar Basin part I: The eastern Luliang Uplift and its link with the East Junggar terrane. *Gondwana Res.* **2015**, *27*, 1089–1109. https://doi.org/10.1016/j.gr.2014.08.015.
120. Li, D.; He, D.F.; Yang, Y.H.; Lian, Y.C. Petrogenesis of mid-Carboniferous volcanics and granitic intrusions from western Junggar Basin boreholes: Geodynamic implications for the Central Asian Orogenic Belt in Northwest China. *Int. Geol. Rev.* **2014**, *56*, 1668–1690. https://doi.org/10.1080/00206814.2014.958766.
121. Li, D.; He, D.F.; Lian, Y.C.; Lu, Y.; Yi, Z.J. Structural evolution and late Carboniferous magmatism of the Zhongguai arc in the western Junggar Basin, Northwest China: Implications for tectonic evolution of the Junggar Ocean. *Int. Geol. Rev.* **2016**, *59*, 1234–1255. https://doi.org/10.1080/00206814.2016.1160801.
122. Li, D.; He, D.F.; Santosh, M.; Ma, D.L. Tectonic framework of the northern Junggar Basin Part II: The island arc basin system of the western Luliang Uplift and its link with the West Junggar terrane. *Gondwana Res.* **2015**, *27*, 1110–1130. https://doi.org/10.1016/j.gr.2014.08.019.

123. Zhang, P. Late Paleozoic Tectonic Transition and Evolution of Paleo-Oceanic Basin in Central West Junggar. Ph.D. Thesis, China University of Geosciences, Wuhan, China, June 2020
124. Chen, S. Late Paleozoic Remnant Ocean Basin and Ophiolitic Mélanges in Strike-Slip Fault Zones in West Junggar, Xinjiang. Ph.D. Thesis, Peking University, Beijing, China, June 2013
125. John, F.H. A Zircon-Tourmaline-Rutile Maturity Index and the Interdependence of the Composition of Heavy Mineral Assemblages with the Gross Composition and Texture of Sandstones. *J. Sediment. Res.* **1962**, *32*, 440–450. https://doi.org/10.1306/74d70ce5-2b21-11d7-8648000102c1865d.
126. Morton, A.C. Heavy Minerals in Provenance Studies. In *Provenance of Arenites*; Zuffa, G.G., Ed.; Springer: Dordrecht, The Netherlands, 1985; Volume 148, pp. 249–277.
127. Morton, A.C.; Hallsworth, C. Stability of Detrital Heavy Minerals During Burial Diagenesis. In *Heavy Minerals in Use*; Mange, M.A., Wright, D.T., Eds.; Developments in Sedimentology; Elsevier: Amsterdam, The Netherlands, 2007; Volume 58, pp. 215–245.
128. Morton, A.C.; Hallsworth, C.R. Processes controlling the composition of heavy mineral assemblages in sandstones. *Sediment. Geol.* **1999**, *124*, 3–29. https://doi.org/10.1016/S0037-0738(98)00118-3.
129. Morton, A.C.; Hallsworth, C. Identifying Provenance-Specific Features of Detrital Heavy Mineral Assemblages in Sandstones. *Sediment. Geol.* **1994**, *90*, 241–256. https://doi.org/10.1016/0037-0738(94)90041-8.
130. Liu, Q.H.; Zhu, H.T.; Shu, Y.; Zhu, X.M.; Yang, X.H.; Chen, L.; Tan, M.X.; Geng, M.Y. Provenance identification and sedimentary analysis of the beach and bar systems in the Palaeogene of the Enping Sag, Pearl River Mouth Basin, South China Sea. *Mar. Pet. Geol.* **2016**, *70*, 251–272. https://doi.org/10.1016/j.marpetgeo.2015.12.002.
131. Han, B.F.; Guo, Z.J.; He, G.Q. Timing of major suture zones in North Xinjiang, China: Constraints from stitching plutons. *Acta Petrol. Sin.* **2010**, *26*, 2233–2246.
132. Duan, F.H.; Li, Y.J.; Zhi, Q.; Yang, G.X.; Gao, J.B. Petrogenesis and geodynamic implications of Late Carboniferous sanukitic dikes from the Bieluagaxi area of West Junggar, NW China. *J. Asian Earth Sci.* **2019**, *175*, 158–177. https://doi.org/10.1016/j.jseaes.2019.01.013.
133. Chen, B.; Zhu, Y.F. Petrology, Geochemistry and Zircon U-Pb Chronology of Gabbro in Darbut Ophiolitic Mélange, Xinjiang. *Acta Petrol. Sin.* **2011**, *27*, 1746–1758.
134. Yang, G.; Xiao, L.; Wang, G.C.; Gao, R.; He, X.X.; Yan, S.W.; Yang, W.; Yan, W.B.; Zhou, P. Geochronology, Geochemistry and Zircon Lu-Hf Study of Granites in Western Section of Xiemisitai Area, Western Junggar. *Earth Sci.* **2015**, *40*, 548-562. https://doi.org/10.3799/dqkx.2015.043.
135. Yang, Y.Q.; Zhao, L.; Xu, Q.Q.; Zheng, R.G.; Liu, J.H.; Zhang, J. Early Paleozoic tectonic evolution of the northern West Junggar (NW China): Constraints from Early Cambrian-Middle Silurian felsic plutons of the Chagantaolegai ophiolitic melange. *Lithos* **2019**, *350*, 105225. https://doi.org/10.1016/j.lithos.2019.105225.
136. Jin, S.; Zhang, H.W.; Han, Y.B.; Li, X.F.; Wang, X.Y.; Wu, L.; Wang, Z.Y. Zircon U-Pb ages and Hf isotopic compostions of Sugensala granite in western section of Xiemisitai area, western Junggar: Constraints on the tectonic evolution. *Geol. China* **2020**, 1–17.
137. Zhang, L.M. Geochemistry Constraints on the Origin and Evolution of the Late Paleozoic Ophiolite in the West Junggar Ph.D. Thesis, Chang'an University, Xi'an, 15 June 2014
138. Wei, R.Z. The Mayileshang Pillow Lavas (Western Junggar, Xinjiang) and their Tectonic Implications: Constraints from the Geological and Geochemical Characteristics and Rb-Sr Isochron Ages. *Xinjiang Geol.* **2010**, *28*, 229–235. https://doi.org/10.3969/j.issn.1000-8845.2010.03.001.
139. Chen, C.Q. Detrital Zircon U-Pb Ages of the Sedimentary Covers on the Barleik Ophiolite in Western Junggar, Xinjiang, and their Geological Significance. BA Thesis, Peking University, Beijing, China, 26 May 2019
140. Sun, H.; Xu, Y.; Han, B.F.; Liao, W.; Li, A.; Chen, C.Q.; Jiang, S.H. Changes in sedimentary environments and provenances of the Carboniferous-Lower Permian strata in Ashelekuoerlesi area, West Junggar. *Geol. Bull. China* **2020**, *39*, 963–982.
141. Wei, Y.J.; He, D.F.; Lei, Z.Y.; Yin, C.; Zhang, L.P.; Hu, S.Y.; Dong, D.Z. Sedimentary Response to the Activity of the Permian Thrusting Fault in the Foreland Thrust Belt of the Northwestern Junggar Basin. *Acta Geol. Sin.* **2004**, *78*, 612–625. https://doi.org/10.3321/j.issn:0001-5717.2004.05.005.
142. He, D.F.; Yin, C.; Du, S.K.; Shi, X.; Ma, H.S. Characteristics of structural segmentation of foreland thrust belts—A case study of the fault belts in the northwestern margin of Junggar Basin. *Earth Sci. Front.* **2004**, *11*, 91-101.
143. Tao, H.F.; Wang, Q.C.; Yang, X.F.; Jiang, L. Provenance and tectonic setting of Late Carboniferous clastic rocks in West Junggar, Xinjiang, China: A case from the Hala-alat Mountains. *J. Asian Earth Sci.* **2013**, *64*, 210–222. https://doi.org/10.1016/j.jseaes.2012.12.019.
144. Shi, T.; Li, Q.; Amuti, A.; Xiao, J.; Liu, F.; Yang, W.; Li, Q.; Zhang, H.; Lü, Z.; Peng, H. Bashkirian taeniate bisaccate pollen-dominated palynological assemblage from northwestern Junggar Basin, Xinjiang Province, China. *Geol. J.* **2021**, *56*, 6031–6042. https://doi.org/10.1002/gj.4167.
145. Tang, Y.; Xu, Y.; Qu, J.H.; Meng, X.C.; Zou, Z.W. Fan-Delta Group Characteristics and Its Distribution of the Triassic Baikouquan Reservoirs in Mahu Sag of Junggar Basin. *Xinjiang Pet. Geol.* **2014**, *35*, 628–635.

146. Fang, S.H.; Jia, C.Z.; Guo, Z.J.; Song, Y.; Xu, H.M.; Liu, L.J. New view on the Permian evolution of the Junggar basin and its implications for tectonic evolution. *Earth Sci. Front.* **2006**, *13*, 108–121. https://doi.org/10.3321/j.issn:1005-2321.2006.03.015.
147. Li, P.L.; Feng, J.H.; Lu, Y.C.; Hao, F. *Structural Sedimentation and Accumulation in Junggar Basin;* Geological Publishing House: Beijing, China, 2010, pp. 1-340.
148. Liu, D.D.; Zhang, C.; Yao, E.D.; Song, Y.; Jiang, Z.X.; Luo, Q. What generated the Late Permian to Triassic unconformities in the southern Junggar Basin and western Turpan Basin; tectonic uplift, or increasing aridity? *Palaeogeogr. Palaeoclimatol. Palaeoecol.* **2017**, *468*, 1–17. https://doi.org/10.1016/j.palaeo.2016.11.045.
149. Jackson, S.E.; Pearson, N.J.; Griffin, W.L.; Belousova, E.A. The application of laser ablation-inductively coupled plasma-mass spectrometry to in situ U–Pb zircon geochronology. *Chem. Geol.* **2004**, *211*, 47–69. https://doi.org/10.1016/j.chemgeo.2004.06.017.
150. Andersen, T. Correction of common lead in U–Pb analyses that do not report Pb-204. *Chem. Geol.* **2002**, *192*, 59–79. https://doi.org/10.1016/s0009-2541(02)00195-x.
151. Yuan, H.L.; Gao, S.; Liu, X.M.; Li, H.M.; Gunther, D.; Wu, F.Y. Accurate U-Pb age and trace element determinations of zircon by laser ablation-inductively coupled plasma-mass spectrometry. *Geostand. Geoanal. Res.* **2004**, *28*, 353–370. https://doi.org/10.1111/j.1751-908X.2004.tb00755.x.